Hematoxylin and eosin-stained (H&E) sections of bone were examined under a light microscope (Fig. 6a). In addition, we also analyzed 4-week samples by use of polarized light microscopy (Fig. 6b), because calcified immature bone tissue cannot be distinguished from collagenous fibrous tissue on decalcified H&E sections until several weeks after bone formation. Non-calcified woven bone is observed as shiny white fibrous tissue under a polarized light microscope [20, 21].

Histological analysis showed clear differences in tissue formation between the different treatment conditions. In the control group, sparse fibrous connective tissue was observed to traverse the empty defects and newly formed bone was only found in the area adjacent to the edges of the defect site 4 weeks after operation. Woven bone was not clearly observed in polarized microscopic images of the defect site. This pattern of bone formation was also observed after 8 and 12 weeks, except that the new bone at the periphery of the bone hole became thicker over time. Twelve weeks after operation, a large bone defect still remained in the control group.

In the CGF group, similar to the control group, only fibrous connective tissue was observed to traverse the defects and newly formed bone was observed at the edges of the defect site only 4 weeks after operation. However, in contrast with the control group, thin woven bone-like tissue was observed within the defects by polarized light microscopic analysis (Fig. 6b, white arrows). Over time, the new bone at the periphery gradually grew upwards to the central area of the defect site. Twelve weeks after operation, newly formed bone covered a large area of the bone defect.

In the CGF + BMSC group, islands of newly formed bone were observed 4 weeks after operation, which corresponded well with the micro-CT data obtained at this time. In contrast with the other two groups, newly formed bone was found both in the periphery and at the center of the defect site at this time. In addition, abundant neovascularization was observed around the new bone. The new bone became thicker over time, and, 12 weeks after the operation the critical-size bone defect was almost closed and bone marrow was confirmed to be present within the new bone tissues, resulting in a structure similar to that of normal cranial tissues.

Discussion

This study demonstrated that CGF, a second-generation platelet concentrate, effectively promoted the repair of bone defects and had particularly strong effects when combined with BMSCs. In a rat calvarial defect model, combined use of CGF and BMSCs almost completely repaired critical-size bone defects within 12 weeks. In addition, the CGF extract promoted the proliferation, osteogenic maturation, and mineralization of mesenchymal stem cells in vitro.

It is well established that in the rat calvarial defect model there is a gradual progression of new bone from the periphery of the bone hole to the center. New bone progresses in this direction because the cells that induce bone formation are mainly supplied from the cut edge of the bone defect. However, in our study, micro-CT and

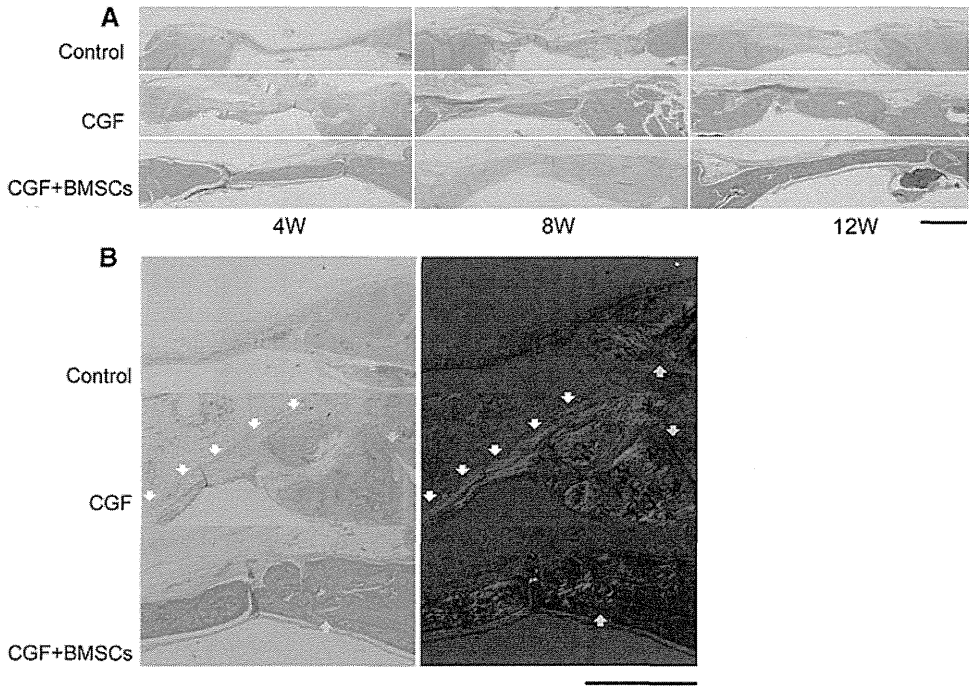

Fig. 6 Treatment of rat calvaria critical-size bone defects with CGF and BMSCs: histological findings. **a** Representative light microscopic images of cranial tissue sections of the three groups, stained with H&E 4, 8, and 12 weeks after operation. (magnification ×20). *Bar* 1,000 μm. **b** Representative light (*left column*) and polarized light (*right column*) microscopic images of H&E stained cranial tissue sections of the three groups 4 weeks after operation, focused on the edges of the cranial holes (magnification ×40). *Bar* 1,000 μm. The *yellow arrows* indicate the edges of the cranial holes. The *white arrows* indicate woven bone tissue (shiny white fibrous tissue)

histological examination revealed new bone formation not only at the periphery of the bone hole but also in the central area of the bone defect in the CGF + BMSCs group, starting 4 weeks after the operation. This new bone included island-shaped new bone that had no contact with the cut edge of the periphery of the bone. Twelve weeks after the operation, critical-size bone defects were almost closed over in the CGF + BMSCs group, whereas large bone defects remained in the control group. This finding suggested that the fibrin network of CGF served as a scaffold for BMSCs that supported the formation of new bone by BMSCs, as reported by Dhohan, Choukroun et al. [2, 22, 23]. In addition, new bone mass significantly increased in the CGF and CGF + BMSCs groups starting 4 weeks after operation, compared with the control group, and this tendency continued until 12 weeks after operation.

Although very favorable results were obtained in these in-vivo experiments, the in-vitro effects of the CGF extract were different depending on the concentration of CGF used. The in-vitro experiments suggested that a highly concentrated CGF extract may inhibit osteogenic maturation and mineralization. Thus, whereas CGF extracts at concentrations between 1 and 10 % promoted cellular proliferation, osteogenic maturation, and mineralization in a dose-dependent manner, the effects of a 20 % CGF extract were inferior to those of the 10 % group, suggesting the existence of optimum doses of CGF. With regard to its effect on *COL1A1* gene expression, expression of this gene decreased in the presence of a high concentration (20 %) of CGF compared with its expression in the control group (0 %), indicating that CGF might actually function to inhibit bone formation. We speculate that this inhibitory effect of CGF might be because, as reported by Dhohan et al. [4], the CGF extract contains not only growth factors favorable for bone formation but also inflammatory cytokines, for example tumor necrosis factor-α (TNF-α) and interleukin-1 (IL-1), which may inhibit bone formation (Fig. 4). Therefore, at a high concentration of CGF the inhibitory action of inflammatory cytokines on bone formation may dominate over the promoting action of the growth factors, which would result in unfavorable effects on bone formation. This concentration-dependent effect seems to be one of the reasons why contradictory effects of PRP on bone formation have been described in previous reports [8–10]. In addition, the results from polymerase chain reaction (PCR) analysis in this study did not reveal any significant change in the expression of such osteogenic master genes as RUNX2 and OSX, which determine whether MSCs are directed toward differentiation into osteoblasts, irrespective of the concentration of CGF extract. These results suggest that the CGF extract stimulates osteogenic maturation only and does not promote commitment of MSCs to osteoblast differentiation.

In this study, we found that CGF served as a good scaffold for BMSCs for treatment of a critical-size bone defect model. The advantages of using CGF as a scaffold are:

1. CGF contains cytokines that promote cell growth, maturation, and matrix production;
2. CGF preparation and cell integration into CGF, are quick and easy; and
3. CGF is safe because it contains nothing but autologous blood ingredients.

For all these reasons we assume CGF will also work as a good scaffold for bone regeneration when it is applied clinically. However, when considering the actual clinical application of combination therapy of CGF and cell transplantation, it will be necessary to optimize the cells to be used (their origin and preparation) and the amount of CGF and other ingredients or modifications that must be applied.

Conclusion

CGF promoted the proliferation, osteogenic maturation, and mineralization of mesenchymal stem cells in vitro, and combination therapy of CGF with BMSCs enabled excellent healing of a critical-size bone defect in vivo. CGF in combination with mesenchymal cell transplantation may be suitable for treatment of large bone defects that are difficult to treat by other methods. However, further research and optimization of the cells and CGF used, and other conditions, are needed before clinical application.

Acknowledgments We thank Dr Junya Toguchida, Kyoto University, for kindly providing the hTERT-E6/E7 cells and Mrs Mari Shinkawa for technical assistance with the histological study. This study was supported by a Grant-in-Aid for Scientific Research (no. 23390364) from the Ministry of Education, Culture, Sports, Science, and Technology, Japan, and by a special research subsidy from Terumo Life Science Foundation. The funders had no role in study design, data collection and analysis, decision to publish, or preparation of the manuscript.

Conflict of interest No competing financial interests exist.

References

1. Mosesson MW, Siebenlist KR, Meh DA. The structure and biological features of fibrinogen and fibrin. Ann N Y Acad Sci. 2001;936:11–30.
2. Dohan DM, Choukroun J, Diss A, Dohan SL, Dohan AJ, Mouhyi J, et al. Platelet-rich fibrin (PRF): a second-generation platelet concentrate. Part I: technological concepts and evolution. Oral Surg Oral Med Oral Pathol Oral Radiol Endod. 2006;101:e37–44.
3. Dohan DM, Choukroun J, Diss A, Dohan SL, Dohan AJ, Mouhyi J, et al. Platelet-rich fibrin (PRF): a second-generation platelet

concentrate. Part II: platelet-related biologic features. Oral Surg Oral Med Oral Pathol Oral Radiol Endod. 2006;101:e45–50.
4. Dohan DM, Choukroun J, Diss A, Dohan SL, Dohan AJ, Mouhyi J, et al. Platelet-rich fibrin (PRF): a second-generation platelet concentrate. Part III: leucocyte activation: a new feature for platelet concentrates? Oral Surg Oral Med Oral Pathol Oral Radiol Endod. 2006;101:e51–5.
5. Brown LF, Lanir N, McDonagh J, Tognazzi K, Dvorak AM, Dvorak HF. Fibroblast migration in fibrin gel matrices. Am J Pathol. 1993;142:273–83.
6. Marx RE, Carlson ER, Eichstaedt RM, Schimmele SR, Strauss JE, Georgeff KR. Platelet-rich plasma: growth factor enhancement for bone grafts. Oral Surg Oral Med Oral Pathol Oral Radiol Endod. 1998;85:638–46.
7. Pietrzak WS, Eppley BL. Platelet rich plasma: biology and new technology. J Craniofacial Surg. 2005;16:1043–54.
8. Plachokova AS, Nikolidakis D, Mulder J, Jansen JA, Creugers NH. Effect of platelet-rich plasma on bone regeneration in dentistry: a systematic review. Clin Oral Implant Res. 2008;19: 539–45.
9. Freymiller EG, Aghaloo TL. Platelet-rich plasma: ready or not? J Oral Maxillofac Surg Off J Am Assoc Oral Maxillofac Surg. 2004;62:484–8.
10. Schmitz JP, Hollinger JO. The biology of platelet-rich plasma. J Oral Maxillofac Surg Off J Am Assoc Oral Maxillofac Surg. 2001;59:1119–21.
11. Dohan Ehrenfest DM, Rasmusson L, Albrektsson T. Classification of platelet concentrates: from pure platelet-rich plasma (P-PRP) to leucocyte- and platelet-rich fibrin (L-PRF). Trends Biotechnol. 2009;27:158–67.
12. Sohn DS, Heo JU, Kwak DH, Kim DE, Kim JM, Moon JW, et al. Bone regeneration in the maxillary sinus using an autologous fibrin-rich block with concentrated growth factors alone. Implant Dent. 2011;20:389–95.
13. Dohan Ehrenfest DM, de Peppo GM, Doglioli P, Sammartino G. Slow release of growth factors and thrombospondin-1 in Choukroun's platelet-rich fibrin (PRF): a gold standard to achieve for all surgical platelet concentrates technologies. Growth Factors (Chur, Switzerland). 2009;27:63–9.
14. He L, Lin Y, Hu X, Zhang Y, Wu H. A comparative study of platelet-rich fibrin (PRF) and platelet-rich plasma (PRP) on the effect of proliferation and differentiation of rat osteoblasts in vitro. Oral Surg Oral Med Oral Pathol Oral Radiol Endod. 2009;108:707–13.
15. Okamoto T, Aoyama T, Nakayama T, Nakamata T, Hosaka T, Nishijo K, et al. Clonal heterogeneity in differentiation potential of immortalized human mesenchymal stem cells. Biochem Biophys Res Commun. 2002;295:354–61.
16. Lucarelli E, Beccheroni A, Donati D, Sangiorgi L, Cenacchi A, Del Vento AM, et al. Platelet-derived growth factors enhance proliferation of human stromal stem cells. Biomaterials. 2003;24:3095–100.
17. Graziani F, Ivanovski S, Cei S, Ducci F, Tonetti M, Gabriele M. The in vitro effect of different PRP concentrations on osteoblasts and fibroblasts. Clin Oral Implant Res. 2006;17:212–9.
18. Weibrich G, Hansen T, Kleis W, Buch R, Hitzler WE. Effect of platelet concentration in platelet-rich plasma on peri-implant bone regeneration. Bone. 2004;34:665–71.
19. Choi BH, Zhu SJ, Kim BY, Huh JY, Lee SH, Jung JH. Effect of platelet-rich plasma (PRP) concentration on the viability and proliferation of alveolar bone cells: an in vitro study. Int J Oral Maxillofac Surg. 2005;34:420–4.
20. Sverzut CE, Lucas MA, Sverzut AT, Trivellato AE, Beloti MM, Rosa AL, et al. Bone repair in mandibular body osteotomy after using 2.0 miniplate system—histological and histometric analysis in dogs. Int J Exp Pathol. 2008;89:91–7.
21. Retamoso LB, Montagner F, Camargo ES, Vitral RW, Tanaka OM. Polarized light microscopic analysis of bone formation after inhibition of cyclooxygenase 1 and 2. Anat Record 2010;293: 195–9.
22. Choukroun J, Diss A, Simonpieri A, Girard MO, Schoeffler C, Dohan SL, et al. Platelet-rich fibrin (PRF): a second-generation platelet concentrate. Part IV: clinical effects on tissue healing. Oral Surg Oral Med Oral Pathol Oral Radiol Endod. 2006; 101:e56–60.
23. Choukroun J, Diss A, Simonpieri A, Girard MO, Schoeffler C, Dohan SL, et al. Platelet-rich fibrin (PRF): a second-generation platelet concentrate. Part V: histologic evaluations of PRF effects on bone allograft maturation in sinus lift. Oral Surg Oral Med Oral Pathol Oral Radiol Endod. 2006;101:299–303.

Hindawi Publishing Corporation
Disease Markers
Volume 35 (2013), Issue 5, Pages 573–579
http://dx.doi.org/10.1155/2013/392578

Hindawi

Research Article

CD90- (Thy-1-) High Selection Enhances Reprogramming Capacity of Murine Adipose-Derived Mesenchymal Stem Cells

Koichi Kawamoto,[1] Masamitsu Konno,[2] Hiroaki Nagano,[2] Shimpei Nishikawa,[2] Yoshito Tomimaru,[2] Hirofumi Akita,[2] Naoki Hama,[2] Hiroshi Wada,[2] Shogo Kobayashi,[2] Hidetoshi Eguchi,[2] Masahiro Tanemura,[3] Toshinori Ito,[4] Yuichiro Doki,[1] Masaki Mori,[1] and Hideshi Ishii[2]

[1] *Department of Surgery, Graduate School of Medicine, Osaka University, 2-2 Yamadaoka, Suita, Osaka 565-0871, Japan*
[2] *Department of Frontier Science for Cancer and Chemotherapy, Graduate School of Medicine, Osaka University, 2-2 Yamadaoka, Suita, Osaka 565-0871, Japan*
[3] *Department of Surgery and Institute for Clinical Research, National Hospital Organization Kure Medical Center and Chugoku Cancer Center, Hiroshima 737-0023, Japan*
[4] *Department of Complementary and Alternative Medicine, Graduate School of Medicine, Osaka University, 2-2 Yamadaoka, Suita, Osaka 565-0871, Japan*

Correspondence should be addressed to Hiroaki Nagano; hnagano@gesurg.med.osaka-u.ac.jp and Hideshi Ishii; hishii@gesurg.med.osaka-u.ac.jp

Received 18 June 2013; Revised 7 September 2013; Accepted 12 September 2013

Academic Editor: Chao Hung Hung

Background. Mesenchymal stem cells (MSCs), including adipose tissue-derived mesenchymal stem cells (ADSC), are multipotent and can differentiate into various cell types possessing unique immunomodulatory features. Several clinical trials have demonstrated the safety and possible efficacy of MSCs in organ transplantation. Thus, stem cell therapy is promising for tolerance induction. In this study, we assessed the reprogramming capacity of murine ADSCs and found that CD90 (Thy-1), originally discovered as a thymocyte antigen, could be a useful marker for cell therapy. *Method.* Murine ADSCs were isolated from B6 mice, sorted using a FACSAria cell sorter by selection of $CD90^{Hi}$ or $CD90^{Lo}$, and then transduced with four standard factors (4F; Oct4, Sox2, Klf4, and c-Myc). *Results.* Unsorted, $CD90^{Hi}$-sorted, and $CD90^{Lo}$-sorted murine ADSCs were reprogrammed using standard 4F transduction. $CD90^{Hi}$ ADSCs showed increased numbers of alkaline phosphatase-positive colonies compared with $CD90^{Lo}$ ADSCs. The relative reprogramming efficiencies of unsorted, $CD90^{Hi}$-sorted, and $CD90^{Lo}$-sorted ADSCs were 100%, 116.5%, and 74.7%, respectively. $CD90^{Hi}$ cells were more responsive to reprogramming. *Conclusion.* $CD90^{Hi}$ ADSCs had greater reprogramming capacity than $CD90^{Lo}$ ADSCs, suggesting that ADSCs have heterogeneous subpopulations. Thus, $CD90^{Hi}$ selection presents an effective strategy to isolate a highly suppressive subpopulation for stem cell-based tolerance induction therapy.

1. Introduction

Induced pluripotent stem (iPS) cells can be directly generated from fibroblast cultures by expression of four factors (4F), including octamer-binding transcription factor 4, sex-determining region Y-box 2, Kruppel-like factor 4, and myelocytomatosis viral oncogene homolog [1]. Although these factors present attractive sources for stem cell therapy, the mechanisms by which they are generated are not fully understood. The inefficiency of iPS cell generation has prompted the development of two contending models, namely, the stochastic and elite models. A recent multilineage-differentiating stress-enduring cell study suggested the greater utility of the elite model over the stochastic model [2]. In either model, stem cells or progenitor cells isolated for experimental or therapeutic research are usually heterogeneous populations; therefore, a more favorable subfraction for use in stem cell therapy may

exist. Indeed, several reports have suggested that the differentiation stage of the starting cell line has a critical influence on the efficiency of reprogramming into iPS cells in hematopoiesis [3]. Immature cell populations, such as lin$^-$c-Kit$^+$Sca1$^+$CD48$^-$CD150$^+$CD34$^-$ (lack of lineage/Hardy-Zuckerman 4 feline sarcoma viral oncogene homolog/spinocerebellar ataxia/cluster of differentiation 48$^-$/150$^+$/34$^-$) hematopoietic stem cells, in general give rise to iPS cells at higher efficiencies than terminally differentiated cell types. Furthermore, a recent study demonstrated that CD90^{Hi} adipose tissue-derived mesenchymal stem cells (ADSCs) are more capable of forming bone both *in vitro* and *in vivo* than in CD105^{Lo} cells [4]. CD90 (Thy-1) is a 25–37-kDa glycosylphosphatidylinositol-anchored glycoprotein expressed mainly in leukocytes that have been used as murine pan T-cell markers, like CD2, CD5, and CD28.

Multipotent mesenchymal stem cells (MSCs), which represent a nonhematopoietic cell population, can differentiate into mesenchymal tissues (i.e., bone, cartilage, or fat) [5, 6]; they were first isolated from bone marrow and later from non-marrow tissues, including umbilical cord blood and adipose tissue [5, 6]. Immunologically, MCSs are known to be less immunogenic because of, at least in part, the lack of surface-expressed human leukocyte antigens [5]. Moreover, they have been shown to possess anti-inflammatory and immunosuppressive effects both in murine and human models of diabetes [7, 8]. Thus, the immunoregulatory properties of MSCs are appealing, because they inhibit T-cell proliferation and differentiation of monocytes to dendritic cells, modulate B-cell functions, and suppress natural killer cell cytotoxicity. Solid organ transplantation is an established and useful treatment option for end-stage organ failure. Despite excellent short-term results, long-term survival of transplanted grafts has not improved accordingly because of graft rejection, graft fibrosis, or side effects of immunosuppressants. The aim of stem cell therapy for solid organ transplantation is to prevent or treat acute rejection and to involve autologous or allogeneic stem cell transplantation into patients, either through local delivery or systemic infusion. Currently, there are over 100 ongoing clinical trials to evaluate the utility of MSCs, especially in kidney transplantation [9–11].

ADSCs have been shown to consist of heterogeneous subpopulations; therefore, we hypothesized that CD90^{Hi} ADSCs might exhibit increased reprogramming capacities and subsequently have better immunoregulatory effects. Hence, the aim of the present study was to compare the reprogramming capacity of sorted murine CD90^{Hi} ADSCs. Our data demonstrated that CD90^{Hi} selection improved the reprogramming capacity of murine ADSCs, suggesting that CD90^{Hi} ADSCs could help prevent graft rejection.

2. Materials and Methods

2.1. ADSC Isolation. Murine ADSCs were isolated from B6 mice as previously described but with slight modifications [7]. Briefly, adipose tissue was obtained from the inguinal fat pads, washed with Dulbecco's phosphate-buffered saline (D-PBS; Invitrogen, Carlsbad, CA, USA) containing 50 U/mL of penicillin and 50 μg/mL of streptomycin (PSM; Invitrogen), and then cut into fine pieces, which were incubated with D-PBS containing 1.0 mg/mL of *Clostridium histolyticum* collagenase (Sigma-Aldrich, St. Louis, MO, USA) in a 37°C shaking incubator for 1 h. The digested tissue was filtered through sterile 70-μm nylon mesh, centrifuged at 430 ×g for 5 min, and resuspended in Dulbecco's modified Eagle's medium (DMEM) (Nacalai Tesque, Kyoto, Japan) supplemented with 10% fetal bovine serum (FBS; HyClone; Thermo Scientific, Waltham, MA, USA) and PSM.

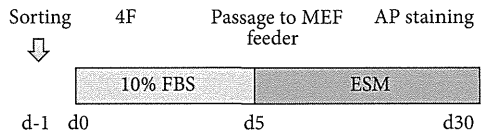

FIGURE 1: Lentiviral-mediated transfer of four iPS cell factor genes in murine ADSCs. A schematic representation of the experiment is shown. Cells were transduced with four factors (4F) after 24 h of incubation. Then, 4F-transduced cells were passaged to MMC-treated MEF feeder cells on day 5. The number of reprogrammed iPS colonies was assessed on posttransduction day 30 by AP staining.

2.2. Cell Sorting. Murine ADSCs were washed with D-PBS and treated with Accutase reagent (EMD Millipore, Billerica, MA, USA) in a 37°C incubator for 2-3 min to dissociate the cells, which were then resuspended in staining media [D-PBS supplemented with FBS (1%) and EDTA (2 mM)]. Next, the cells were stained with fluorescein isothiocyanate-conjugated anti-mouse CD34 (eBioscience, San Diego, CA, USA), phycoerythrin-conjugated anti-mouse CD31, eFluor450 anti-mouse CD45, and allophycocyanin-conjugated anti-mouse CD90.2 for 60 min at 4°C. The cells were then washed with staining media, stained with 7-aminoactinomycin D to exclude dead cells, and sorted using the FACSAria cell sorter (Bio-Rad, Hercules, CA, USA) [12]. The particular phenotypic subsets of CD90^{Hi} and CD90^{Lo} ADSCs, based on CD31, CD45, and CD90 expression, were evaluated by multicolor analysis and sorted by adequate gating.

2.3. Lentiviral Preparation. To prepare the lentiviruses, human embryonic kidney (HEK)-293Ta cells were cultured in DMEM supplemented with 10% FBS and PSM. Then, the cells were seeded at 5.0×10^6 cells per 100 mm dish 1 day before viral transduction. Fugene 6 transfection reagent (22.5 μL; Promega, Madison, WI, USA) was diluted with 500 μL of DMEM and incubated for 5 min at room temperature. Plasmid DNA (2.5 μg) was added to the mixture, which was incubated for an additional 15 min at room temperature. Then, the culture media was replaced with fresh DMEM supplemented 10% FBS and the DNA/Fugene 6 mixture was added dropwise onto the HEK-293Ta cells. The medium was replaced after 24 h. After an additional 48 h, virus-containing supernatants, derived from the HEK-293Ta cultures, were filtered through a 0.22-μL cellulose–acetate filter and analyzed without being frozen.

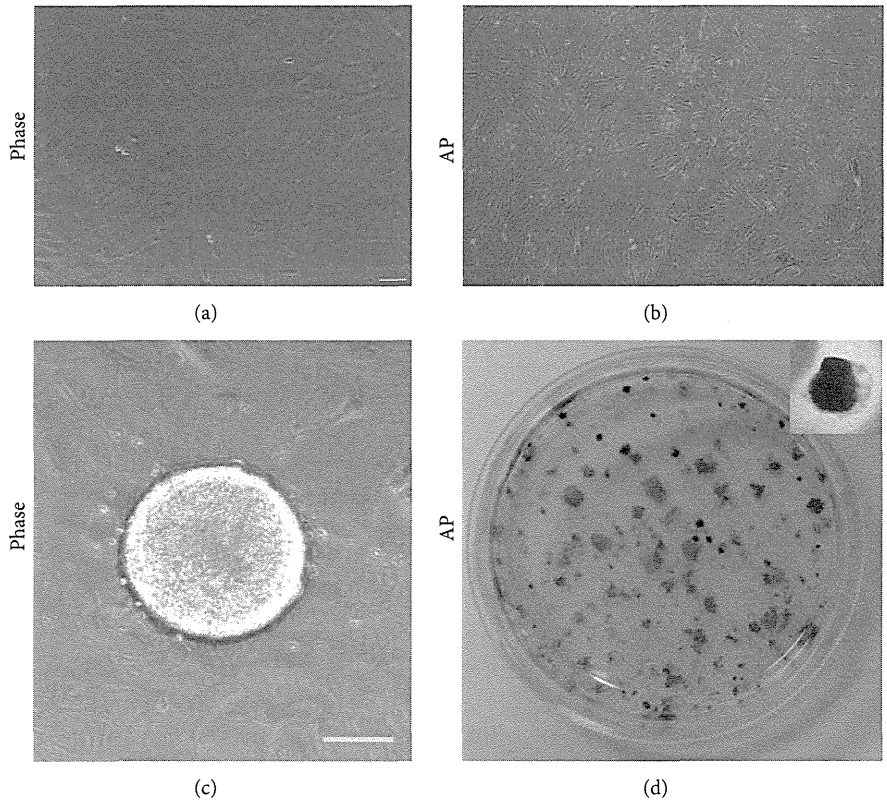

FIGURE 2: 4F transduction resulted in iPS colony formation in unsorted murine ADSCs. Phase (a and c) and AP staining (b and d) of pre- and post- (c and d) transduction were shown.

2.4. Lentiviral Transduction. Sorted $CD90^{Hi}$ and $CD90^{Lo}$ cells were plated onto 6-well culture plates at a density of 1.0×10^5 cells/well, respectively. After incubation for 24 h, the culture medium was retrieved and viral supernatants were added to each well. The next day, the cells were washed with complete medium three times. Mouse embryonic fibroblasts (MEFs) were mitotically inactivated by the addition of 10 μg/mL of mitomycin C (MMC; Nacalai Tesque Inc., Kyoto, Japan) for 90 min and then washed with D-PBS three times. The cells were then cultured with complete medium for at least 2 h, trypsinized, counted, and plated on gelatin-coated 60 mm dishes at a density of 5.0×10^5 cells/well. On posttransduction day 5, the cells were trypsinized; suspended in DMEM supplemented with 15% (v/v) FBS, PSM, 1-mM sodium pyruvate (Invitrogen), 10^{-4} M 2-mercaptoethanol (Nacalai Tesque, Inc.), nonessential amino acid solution, and 1,000 U/mL of leukemia inhibitory factor; after which they were counted. Then, 1000 cells were transferred to MMC-treated MEF feeder cells. On post-transduction day 30, alkaline phosphatase (AP) staining was performed to assess reprogramming efficiency.

2.5. AP Staining. 4F-transduced ADSCs were stained using an AP staining kit (Muto Pure Chemicals, Tokyo, Japan) following the manufacturer's recommended protocol. Briefly, cultured cells were rinsed twice with D-PBS and then fixed for 5 s in ice-cold methanol. Then, the cells were washed with tap water, stained with AP solution at 37° for 120 min, and washed again with running water. The number of AP^+ colonies were manually inspected and counted.

3. Results

Figure 1 describes the experimental protocol used in this study. First, we evaluated the reprogramming capacity of unsorted ADSCs. As shown in Figure 2, parental ADSC showed no colonies and AP staining was negative (negative control). However, 4F transduction resulted in ADSC colony formation. After culturing for 30 days, the cells were stained with AP to test iPS cell pluripotency. AP staining was positive in all colonies. These results clearly demonstrated that murine ADSCs can be reprogrammed using standard 4F. Next we used sorted ADSCs to assess the reprogramming capacities of $CD90^{Hi}$ and $CD90^{Low}$ ADSCs. As shown in Figure 3(a), the CD90 marker was widely expressed on the surfaces of the $CD31^-CD45^-CD34^-$ADSCs. After 24 h of incubation, sorted $CD90^{Hi}$ or $CD90^{Lo}$ ADSCs became attached to the culture dishes (Figure 3(b)) and both showed similar morphologies. Next, we assessed the effect of *in vitro* culture. As shown in Figure 4(a), 7-day culture resulted in the reexpression of CD90 even after sorted $CD90^{Lo}$ ADSCs. These results suggest that sorted cells might be transduced as soon as possible.

To show the successful induction of the undifferentiated state, we employed immunocytochemistry of Oct4

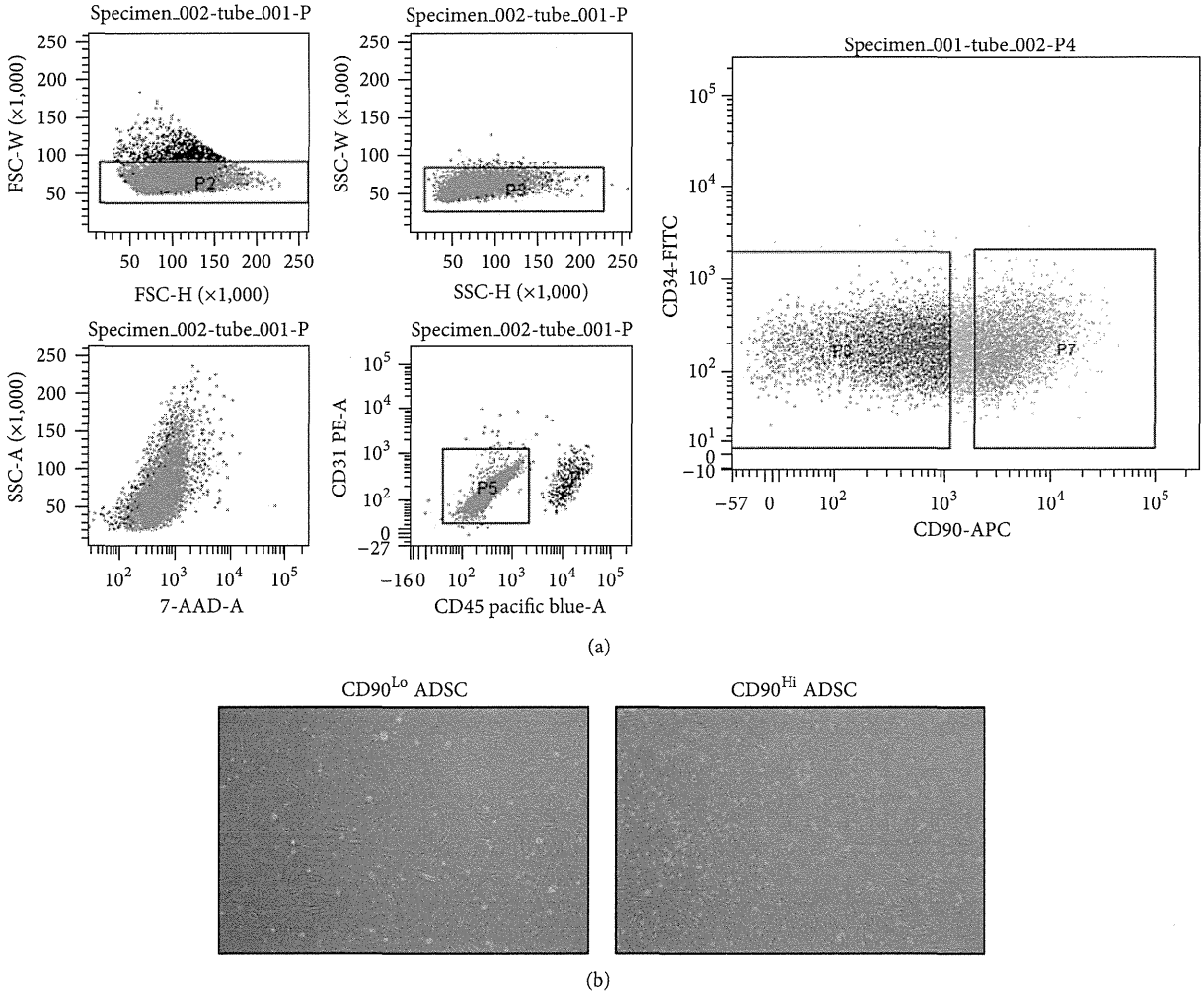

FIGURE 3: CD90^{Hi} and CD90^{Lo} sorting. (a) Gates for CD90^{Hi} (P7) and CD90^{Lo} (P8) are shown. (b) Sorted cells showed similar morphologies 24 h after sorting. Then, the cells were transduced with 4F.

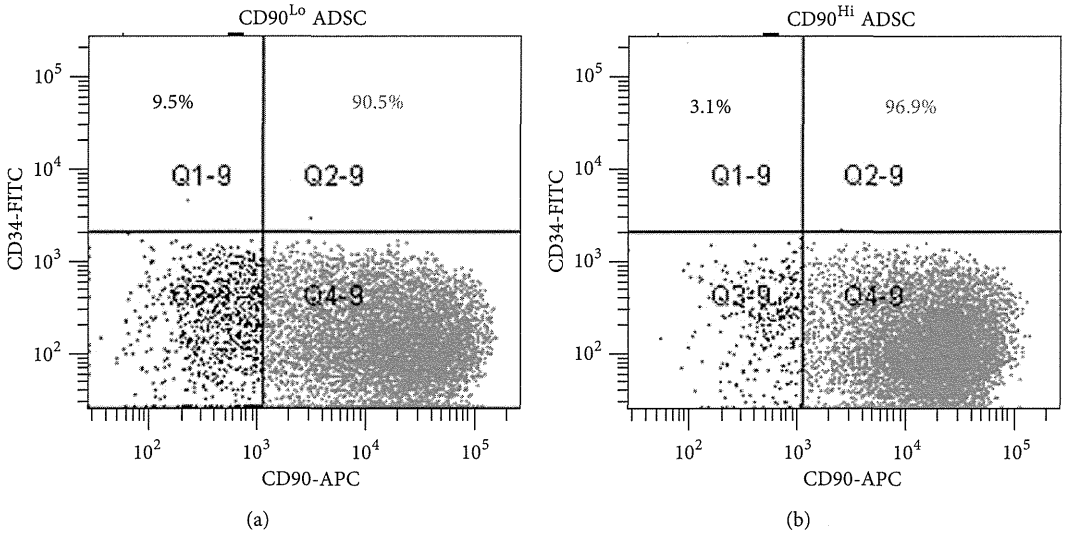

FIGURE 4: Phenotypical analysis after *in vitro* culture of sorted ADSCs.

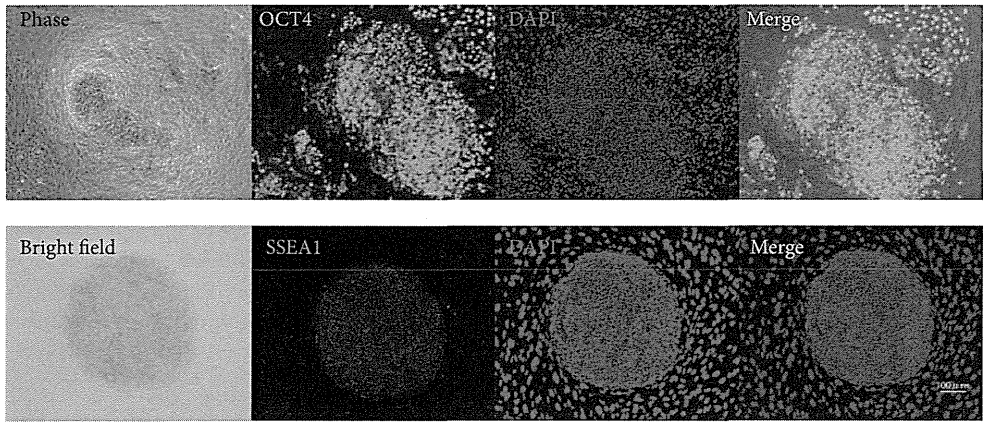

FIGURE 5: Immunocytochemistry of iPS colonies.

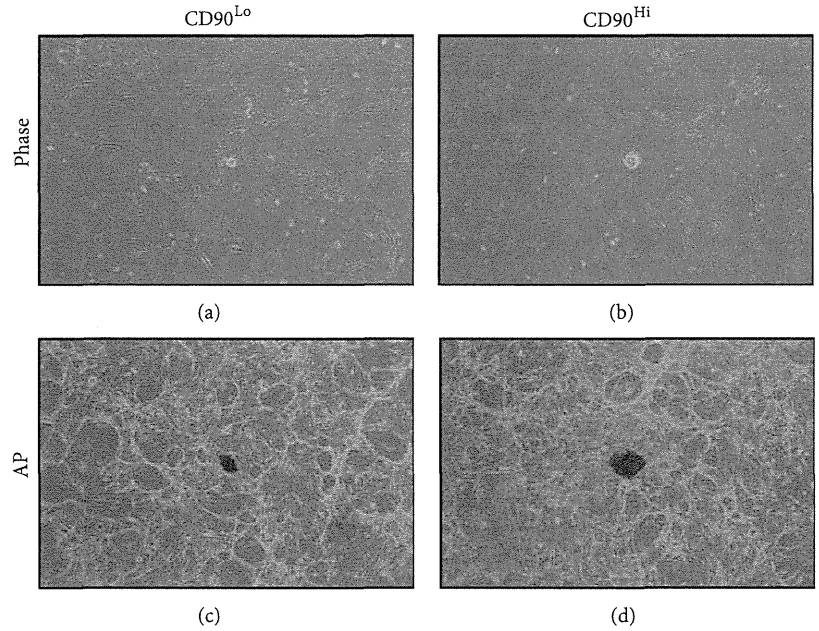

FIGURE 6: Colony formation of the sorted cells. Phase (a and b) and alkaline phosphatase staining (c and d) of $CD90^{Lo}$ (a and c) and $CD90^{Hi}$ (b and d) are shown.

and SSEA1. As shown in Figure 5, colonies were positive for Oct4 and SSEA1. Sorted and 4F-transduced ADSCs also exhibited colony formation. As shown in Figures 6(a) and 6(b), morphologically distinct colonies were visible in both $CD90^{Hi}$ and $CD90^{Lo}$ 4F-transduced ADSCs on posttransduction day 14. On posttransduction day 30, the colonies were stained with AP. There were AP+ colonies in both groups, although the $CD90^{Hi}$ ADSCs tended to form larger colonies than $CD90^{Lo}$ ADSCs (Figures 4(c) and 4(d)). As shown in Figure 7, $CD90^{Hi}$ ADSCs exhibited more AP+ colonies than $CD90^{Lo}$ ADSCs. The reprogramming efficiencies of unsorted, $CD90^{Hi}$-sorted, and $CD90^{Lo}$-sorted ADSCs were 100%, 116.5%, and 74.7%, respectively.

4. Discussion

In the present study, we demonstrated that murine ADSCs can be reprogrammed by standard 4F transduction. Furthermore, iPS cell formation was also observed in CD90-based sorted cells and the $CD90^{Hi}$ sorting resulted in enhanced reprogramming capacity of murine ADSCs compared with $CD90^{Lo}$ ADSCs with regard to colony number. Moreover, there was a trend in the association between CD90 expression level and individual colony size. These results clearly demonstrated that ADSCs have heterogeneous subpopulations and that the $CD90^{Hi}$ ADSCs present favorable candidates for the application of clinical stem cell therapy.

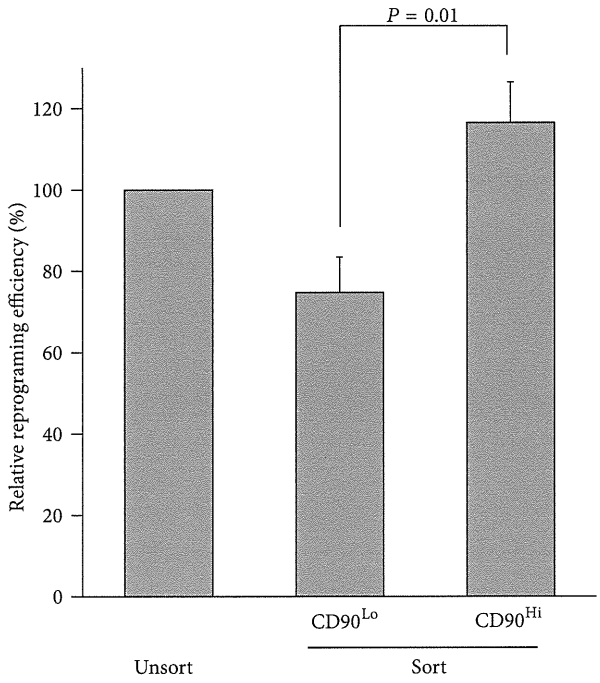

FIGURE 7: Relative reprogramming efficiency of sorted cells compared with unsorted controls.

The importance of CD90 in oncogenesis or properties of cancer stem cells has been reported [13]. CD90 expression reportedly has prognostic values in esophageal squamous cell carcinoma (ESCC) patients, because higher CD90 expression was significantly associated with a strong family history of ESCC and higher incidences of lymph node metastasis. However, the importance of CD90 expression in MSCs has not been fully elucidated; therefore, our next project is to clarify the mechanisms of CD90-mediated immunomodulatory effects. Of note, recent study reported that CD90-expressing niche stromal cells would support hematopoiesis [14].

Stem cell therapy for autoimmune disease is also well described. In a murine inflammatory bowel disease model, ADSCs alleviated experimental colitis by inhibiting inflammatory and autoimmune responses [15]. In mice, Thy-1 is also expressed by thymocytes, peripheral T cells, myoblasts, epidermal cells, and keratinocytes.

We and others previously reported that it is possible to reprogram murine and human cells to pluripotency by direct transfection of mature double-stranded microRNAs without viral vectors [16–18]. These viral-free strategies present effective methods for future stem cell therapy.

Currently, studies are underway to compare the immunoregulatory properties of viral-free strategies both *in vitro* and *in vivo*.

Acknowledgment

Lentiviral vectors (CSII-CMV-mOct3/4-IRES2-Venus, CSII-CMV-mSox2-IRES2-Venus, CSII-CMV-mKlf4-IRES2-Venus, CSII-CMV-mcMyc-IRES2-Venus, pCAG-HIVgp, and pCAG-VSV-G-RSV-Rev) were kindly provided by the Hiroyuki Miyoshi (RIKEN; The Institute of Physical and Chemical Research, Tsukuba, Japan).

References

[1] K. Takahashi and S. Yamanaka, "Induction of pluripotent stem cells from mouse embryonic and adult fibroblast cultures by defined factors," *Cell*, vol. 126, no. 4, pp. 663–676, 2006.

[2] S. Wakao, M. Kitada, Y. Kuroda et al., "Multilineage-differentiating stress-enduring (Muse) cells are a primary source of induced pluripotent stem cells in human fibroblasts," *Proceedings of the National Academy of Sciences of the United States of America*, vol. 108, no. 24, pp. 9875–9880, 2011.

[3] S. Eminli, A. Foudi, M. Stadtfeld et al., "Differentiation stage determines potential of hematopoietic cells for reprogramming into induced pluripotent stem cells," *Nature Genetics*, vol. 41, no. 9, pp. 968–976, 2009.

[4] M. T. Chung, C. Liu, J. S. Hyun et al., "CD90 (Thy-1)-positive selection enhances osteogenic capacity of human adipose-derived stromal cells," *Tissue Engineering A*, vol. 19, pp. 989–997, 2013.

[5] K. Le Blanc and D. Mougiakakos, "Multipotent mesenchymal stromal cells and the innate immune system," *Nature Reviews Immunology*, vol. 12, no. 5, pp. 383–396, 2012.

[6] M. Konno, A. Hamabe, S. Hasegawa et al., "Adipose-derived mesenchymal stem cells and regenerative medicine," *Development, Growth and Differentiation*, vol. 55, pp. 309–318, 2013.

[7] Y. Ohmura, M. Tanemura, N. Kawaguchi et al., "Combined transplantation of pancreatic islets and adipose tissue-derived stem cells enhances the survival and insulin function of islet grafts in diabetic mice," *Transplantation*, vol. 90, no. 12, pp. 1366–1373, 2010.

[8] T. Y. Yeung, K. L. Seeberger, T. Kin et al., "Human mesenchymal stem cells protect human islets from pro-inflammatory cytokines," *PLoS ONE*, vol. 7, Article ID e38189, 2012.

[9] J. Tan, W. Wu, X. Xu et al., "Induction therapy with autologous mesenchymal stem cells in living-related kidney transplants: a randomized controlled trial," *Journal of the American Medical Association*, vol. 307, no. 11, pp. 1169–1177, 2012.

[10] Y. Peng, M. Ke, L. Xu et al., "Donor-derived mesenchymal stem cells combined with low-dose tacrolimus prevent acute rejection after renal transplantation: a clinical pilot study," *Transplantation*, vol. 95, pp. 161–168, 2013.

[11] M. E. Reinders, J. W. de Fijter, H. Roelofs et al., "Autologous bone marrow-derived mesenchymal stromal cells for the treatment of allograft rejection after renal transplantation: results of a phase I study," *Stem Cells Translational Medicine*, vol. 2, pp. 107–111, 2013.

[12] S. Nishikawa, M. Konno, A. Hamabe et al., "Aldehyde dehydrogenase high gastric cancer stem cells are resistant to chemotherapy," *International Journal of Oncology*, vol. 42, pp. 1437–1442, 2013.

[13] K. H. Tang, Y. D. Dai, M. Tong et al., "A CD90(+) tumor-initiating cell population with an aggressive signature and metastatic capacity in esophageal cancer," *Cancer Research*, vol. 73, pp. 2322–2332, 2013.

[14] C. K. Chan, P. Lindau, W. Jiang et al., "Clonal precursor of bone, cartilage, and hematopoietic niche stromal cells," *Proceedings of the National Academy of Sciences of the United States of America*, vol. 110, no. 31, pp. 12643–12648, 2013.

[15] M. A. González, E. Gonzalez-Rey, L. Rico, D. Büscher, and M. Delgado, "Adipose-derived mesenchymal stem cells alleviate experimental colitis by inhibiting inflammatory and autoimmune responses," *Gastroenterology*, vol. 136, no. 3, pp. 978–989, 2009.

[16] K. Okita, M. Nakagawa, H. Hyenjong, T. Ichisaka, and S. Yamanaka, "Generation of mouse induced pluripotent stem cells without viral vectors," *Science*, vol. 322, no. 5903, pp. 949–953, 2008.

[17] N. Miyoshi, H. Ishii, H. Nagano et al., "Reprogramming of mouse and human cells to pluripotency using mature microRNAs," *Cell Stem Cell*, vol. 8, no. 6, pp. 633–638, 2011.

[18] F. Anokye-Danso, C. M. Trivedi, D. Juhr et al., "Highly efficient miRNA-mediated reprogramming of mouse and human somatic cells to pluripotency," *Cell Stem Cell*, vol. 8, no. 4, pp. 376–388, 2011.

Aldehyde dehydrogenase^{high} gastric cancer stem cells are resistant to chemotherapy

SHIMPEI NISHIKAWA[1,2], MASAMITSU KONNO[1], ATSUSHI HAMABE[1,2], SHINICHIRO HASEGAWA[1,2], YOSHIHIRO KANO[1,2], KATSUYA OHTA[1,2], TAKAHITO FUKUSUMI[1,3], DAISUKE SAKAI[1], TOSHIHIRO KUDO[1], NAOTSUGU HARAGUCHI[2], TAROH SATOH[1], SHUJI TAKIGUCHI[2], MASAKI MORI[2], YUICHIRO DOKI[2] and HIDESHI ISHII[1]

Departments of [1]Frontier Science for Cancer and Chemotherapy, [2]Gastroenterological Surgery and [3]Otorhinolaryngology - Head and Neck Surgery, Osaka University Graduate School of Medicine, Suita, Osaka 565-0871, Japan

Received November 2, 2012; Accepted December 10, 2012

DOI: 10.3892/ijo.2013.1837

Abstract. Cancer stem cells (CSCs) are known to influence chemoresistance, survival, relapse and metastasis. Aldehyde dehydrogenase (ALDH) functions as an epithelial CSC marker. In the present study, we investigated the involvement of ALDH in gastric CSC maintenance, chemoresistance and survival. Following screening for eight candidate markers (CD13, CD26, CD44, CD90, CD117, CD133, EpCAM and ALDH), five gastric cancer cell lines were found to contain small subpopulations of high ALDH activity (ALDH^{high} cells). We also examined the involvement of ALDH^{high} cell populations in human primary tumor samples. Immunodeficient NOD/SCID mice were inoculated with tumor tissues obtained from surgical specimens. ALDH^{high} cells were found to persist in the xenotransplanted primary tumor samples. In the immunodeficient mice, ALDH^{high} cells exhibited a greater sphere-forming ability *in vitro* and tumorigenic potential *in vivo*, compared with subpopulations of low ALDH activity (ALDH^{low} cells). Cell cultures treated with 5-fluorouracil and cisplatin exhibited higher numbers of ALDH^{high} cells. *Notch1* and *Sonic hedgehog (Shh)* expression was also found to increase in ALDH^{high} cells compared with ALDH^{low} cells. Therefore, it can be concluded that ALDH generates chemoresistance in gastric cancer cells through *Notch1* and *Shh* signaling, suggesting novel treatment targets.

Correspondence to: Professor M. Mori, Department of Gastroenterological Surgery, Osaka University Graduate School of Medicine, 2-2 Yamadaoka, Suita, Osaka 565-0871, Japan
E-mail: mmori@gesurg.med.osaka-u.ac.jp

Professor Hideshi Ishii, Department of Frontier Science for Cancer and Chemotherapy, Osaka University Graduate School of Medicine, 2-2 Yamadaoka, Suita, Osaka 565-0871, Japan
E-mail: hishii@gesurg.med.osaka-u.ac.jp

Key words: gastric cancer, cancer stem cells, chemotherapy resistance, aldehyde dehydrogenase

Introduction

The discovery of cancer stem cells (CSCs) in hematopoietic malignancies (1) has revealed that tumor tissues comprise a bulk of proliferating or differentiated tumor cells derived from small populations of self-renewing cells (2). Since their identification in leukemia, CSCs have been detected in solid tumors of the head and neck (3), gastrointestinal system (4), colon (5,6), breast (7) and brain (8,9). CSCs are tumorigenic, which is evident from xenotransplantation in immunodeficient mice, and are resistant to chemoradiation, whereas daughter cells are chemoradiation-sensitive (10,11). Recent studies have demonstrated that CSCs survive chemo- and radiation therapy in hypoxic regions of tumors (10,11). Studies of cell-autonomous mechanisms have revealed the involvement of anaerobic glycolysis in CSC maintenance and chemoradiation resistance (10,11). For example, CD13/aminopeptidase N, a liver CSC marker, regulates reactive oxygen species (ROS) through recycling reduced glutathione (GSH), thus contributing to intracellular ROS decrease following chemoradiation exposure (12). Similarly, intracellular ROS are suppressed after chemoradiation therapy through the activity of the hyaluronic acid receptor, CD44, an adhesion molecule expressed in cancer stem-like cells that directly interacts with pyruvate kinase M2, which is putatively involved in anaerobic glycolysis in CSCs (13). Furthermore, the CD44 variant (CD44v) has been shown to interact with xCT, a glutamate-cystine transporter, and to control intracellular GSH levels (14). CD44 abrogation has been shown to cause a loss of xCT from the cell surface, to suppress tumor growth in a transgenic gastric cancer (GC) mouse model and stimulate the p38 (mitogen-activated protein kinase) pathway (a downstream target of ROS) and the expression of the cell cycle inhibitor, p21(CIP1/WAF1), suggesting that CD44 plays a role in GSH synthesis and protection against ROS in gastrointestinal cancers (14). Taken together, these data indicate that cancer metabolism is critical for the initiation and progression of gastrointestinal CSCs.

In the present study, we investigated cell surface markers in gastric CSCs and after screening eight candidate markers

(CD13, CD26, CD44, CD90, CD117, CD133, EpCAM and ALDH), we confirmed the involvement of aldehyde dehydrogenase (ALDH) in sphere formation, tumorigenicity and chemoresistance. Throughout the study of the ALDH pathway, a cancer metabolism regulator, we encountered stemness genes, suggesting novel molecular therapeutic targets.

Materials and methods

Cell lines and cell culture. The human GC cell lines, AGS, NUGC3, GSU, MKN1, MKN7, MKN28, MKN45 and MKN74, were cultured in RPMI-1640 medium (Sigma), supplemented with penicillin, streptomycin and 10% fetal bovine serum, in plastic culture dishes (Corning). Spheres were cultured in Gibco® Dulbecco's modified Eagle's medium with nutrient mixture F-12 (Invitrogen), supplemented with 20 ng/ml human recombinant epidermal growth factor (Promega), 20 ng/ml basic fibroblast growth factor (PeproTech Inc.), B-27® Supplement (Invitrogen) and N2 Supplement (Wako), in low-attachment dishes (Corning).

Cell staining and flow cytometry. Cultured cells were harvested and stained using an Aldefluor® stem cell detection kit (StemCell Technologies) for 45 min at 37˚C. To stain cell surface markers, cells were incubated on ice with antibodies against CD44, CD26, CD117, CD90 (all from BD Biosciences), EpCAM (BioLegend) and CD133 (Miltenyi). Isotype antibodies were used as the negative controls. Discrimination between live and dead cells was carried out using the Live/Dead® Fixable Yellow Dead Cell Stain kit (Invitrogen). Mouse cells were identified by anti-H2kd (eBioscience) and anti-mouse CD45 (eBioscience) antibodies.

Primary surgical specimens and xenografts. Tumor tissues were digested into single cells with collagenase (Roche) and DNase (Worthington) at 37˚C for 1 h. Staining for fluorescence-activated cell sorting (FACS) analysis was performed, as described above. For xenografting, cells were injected subcutaneously with Matrigel® into NOD/SCID mice. All the animal experiments were performed with approval of Animal Experiments Committee of Osaka University.

RNA extraction, cDNA synthesis and quantitative PCR. Total RNA was extracted using TRIzol® reagent. cDNA was synthesized using SuperScript® (Invitrogen). Quantitative PCR was performed using LightCycler® 480 Real-Time PCR system. All procedures were performed according to the manufacturer's instructions.

Statistical analysis. Statistical significance was determined using the Student's t-test. Analyses were performed using JMP software.

Results

Screening of CSC markers in GC cell lines. We examined novel markers in gastric CSCs, if: i) they had been previously reported in other tumor types and for which useful antibodies were available for FACS analysis; ii) they were expressed in small populations (<50%) in the cell lines; and iii) these observations were evident in more than half the cell lines.

We investigated the functions of cell surface markers and intracellular molecules (ALDH) to establish a functional detection system. We screened six GC cell lines (AGS, NUGC3, GSU, MKN7, MKN1 and MKN45) for gastric CSC markers using eight candidate markers expressed in other CSCs (CD13, CD26, CD44, CD90, CD117, CD133, EpCAM and ALDH) (11). As shown in Table I, FACS analysis revealed a high expression of EpCAM in all the cell lines (almost 100% postive cells), whereas CD90, CD117 and CD133 expression was uniformly undetectable or negative. CD26 expression was positive (>50%) in four of the cell lines, but undetectable or negative in the other two, suggesting that CD26 expression depends on individual cell lines rather than the heterogeneous conditions of cell line subpopulations. CD13 expression was detected in only one cell line, GSU. Conversely, the investigation of ALDH indicated that the proportion of cells highly expressing ALDH (ALDH^{high} cells) was relatively small (6.2-45.5%) compared with the other markers (CD13, CD26, CD90, CD117, CD133 and EpCAM; Table I and Fig. 1A). Moreover, the ALDH^{high} cell populations reproducibly disappeared upon the addition of the ALDH inhibitor, diethylaminobenzaldehyde (DEAB), indicating the specificity of detection in ALDH^{high} cell populations. Reportedly, ALDH1A1, a substrate for DEAB inhibition, has been shown to be responsible for ALDH activity in CSCs (15). Thus, we focused on ALDH activity.

Cells expressing high levels of ALDH also express CD44. We examined CD44 expression, reportedly a CSC marker in breast, colon, esophageal and gastric cancers (11,13,14). Two-dimensional analysis data indicated that ALDH^{high} cell populations represented only a small subpopulation of CD44-positive cells, suggesting that ALDH is a good candidate as a CSC marker in GC (Table 1 and Fig. 1B).

Cells expressing high ALDH exist in xenografts in immunodeficient mice. We then examined the involvement of ALDH^{high} cell populations in human primary tumor samples. Primary tumor tissues from surgical specimens were obtained with written informed consent and inoculated into immunodeficient NOD/SCID mice. Approximately 30% of inoculated primary samples formed tumors in the mice after several weeks. The probability of tumor formation is likely influenced by tumor tissue viability (nutrients, necrosis and therapy-related damage), vasculogenesis in the mice (dependent on local conditions) and CSC conditions within primary samples. The tumor sample from a patient was subjected to FACS analysis. The data indicated that 57% of the human living tumor cells (separated by FACS using the Live/Dead Fixable Yellow Dead Cell Stain system and distinguished from mouse cells using anti-H2kd and CD45 antibodies) expressed active ALDH (Fig. 1C), indicating that ALDH^{high} cells are present in primary human tumor sample.

Sphere formation and tumorigenicity of populations expressing high levels of ALDH. We then examined stemness in ALDH^{high} cells. A culture of FACS-sorted ALDH^{high} cells in serum-free medium resulted in the frequent formation of large spheres compared with cells expressing low ALDH (ALDH^{low} cells; Fig. 2A and B), suggesting that ALDH^{high} cells possess a greater self-renewal ability, a critical charac-

Table I. Screening for common CSC markers using six GC cell lines.

	ALDH	CD44	EpCAM	CD133	CD13	CD26	CD90	CD117
AGS	-	+	++	-	-	-	-	-
GSU	+	++	++	-	++	++	-	-
NUGC3	+	+	++	-	-	-	-	-
MKN1	+	++	++	-	-	++	-	-
MKN7	+	++	++	-	-	++	-	-
MKN45	+	++	++	-	-	++	-	-

-, <1%. +, <50%. ++, 50-100%.

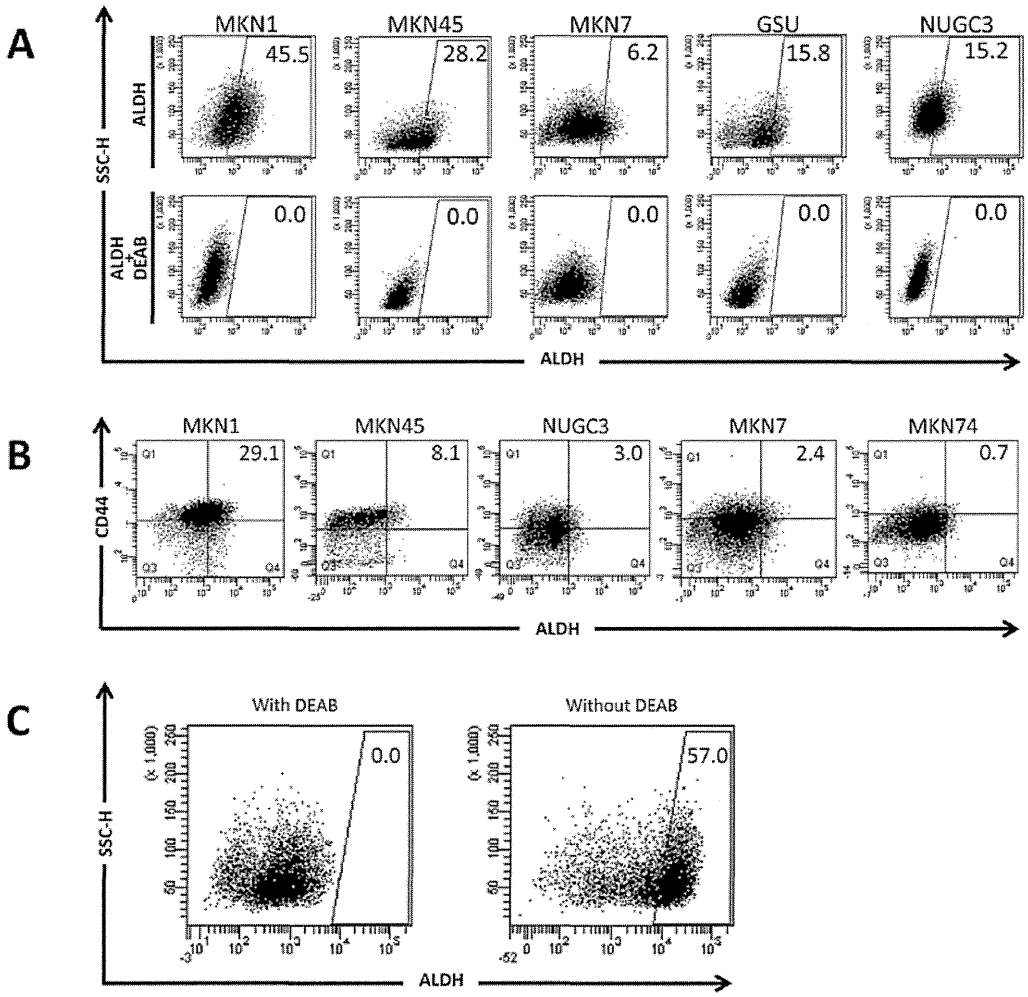

Figure 1. Aldehyde dehydrogenase (ALDH) and the other marker expression in gastric cancer cell lines. (A) ALDH in five gastric cancer (GC) cell lines. Diethylaminobenzaldehyde (DEAB) was used to inhibit ALDH activity, to show the specificity of detection. (B) Double detection of CD44 and ALDH in GC cells. $ALDH^{high}$ cells are a small fraction of $CD44^{+}$ cells. (C) Study of human primary GCs. NOD/SCID mouse xenografted tumor contains $ALDH^{high}$ cells.

teristic of CSCs (2,11). We examined tumorigenicity *in vivo* by inoculating FACS-sorted $ALDH^{high}$ and $ALDH^{low}$ MKN45 cells subcutaneously into NOD/SCID mice. We performed a limiting dilution experiment by reducing the number of inoculating cells. The inoculation of 500 $ALDH^{high}$, but not $ALDH^{low}$ cells resulted in tumor formation in three out of four mice (Fig. 2C). The inoculation of 5,000 cells resulted in tumors being formed from the $ALDH^{high}$ and $ALDH^{low}$ cells (Fig. 2C). Taken together, these observations indicate that, although multiple factors may be involved, ALDH function is closely associated with the initiation, maintenance and progression of CSCs *in vitro* and *in vivo*.

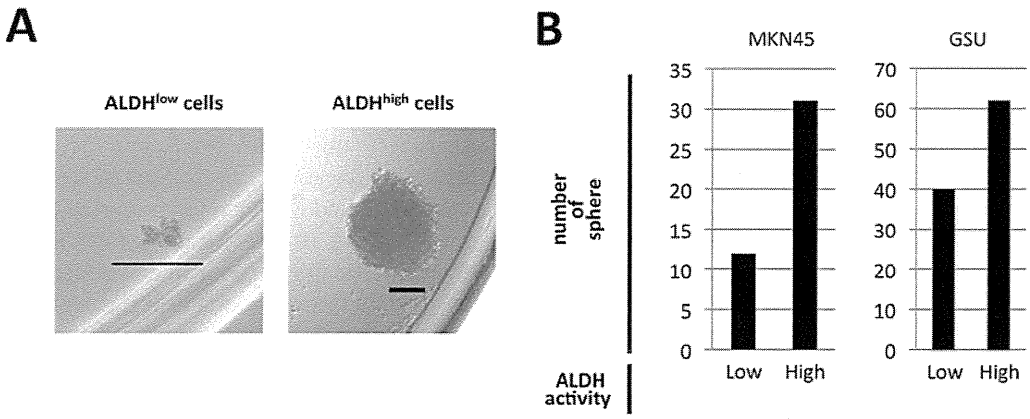

number of transplanted cell	ALDH^{low}	ALDH^{high}
50	0/4	0/4
500	0/4	3/4
5000	3/4	4/4

Figure 2. Sphere formation and tumorigenicity of cells expressing high and low aldehyde dehydrogenase (ALDH). (A) Representative images of sphere formation assay in MKN45 cells. After sorting ALDH^{high} and ALDH^{low} cells, they were subjected to sphere formation assay. Scale bar, 200 μm. (B) Number of spheres formed by ALDH^{high} and ALDH^{low} MKN45 and GSU cells. (C) Tumorigenicity in NOD/SCID mice. The numbers of mice that formed MKN45 tumors are shown.

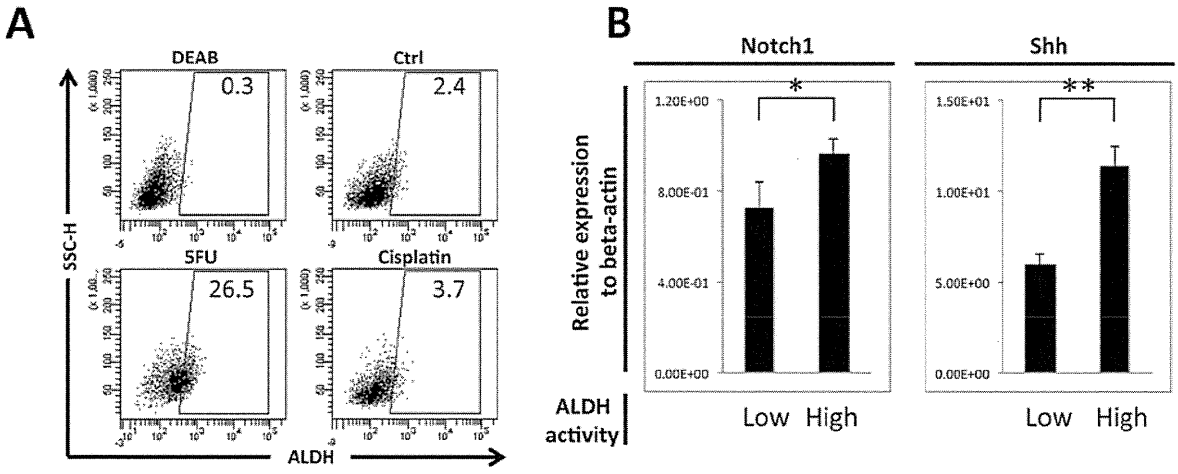

Figure 3. Chemosensitivity and the underlying mechanisms in cells showing high and low expression of aldehyde dehydrogenase (ALDH). (A) Activity of ALDH following exposure to chemotherapeutic agents. ALDH activity was assessed by fluorescence-activated cell sorting after MKN28 cells were cultured in medium containing cisplatin or 5-fluorouracil. (B) Expression of *Notch1* and *Sonic hedgehog (Shh)*. Quantitative reverse transcription PCR was used to detect the higher expression of *Notch1* and *Shh* in ALDH^{high} MKN45 cells. *P<0.05, **P<0.01.

Chemoresistance in cells highly expressing ALDH and the underlying mechanisms. Our aim was the identification of novel molecular therapeutic targets. Reportedly, CSCs can survive toxic injuries and chemoradiation therapy (2,10,11). To combat this, we explored the effect of chemotherapeutic agents commonly used to treat GC. The exposure of the cell cultures to cisplatin and 5-fluorouracil (5-FU) increased the number of ALDH^{high} cells (3.1-4.4% with cisplatin and 31.0% with 5-FU treatment; Fig. 3A), indicating that exposure to these chemotherapeutic agents causes an accumulation of surviving ALDH^{high} CSCs. To elucidate the molecular mechanisms underlying this chemoresistance, we examined gene expression changes in candidate pathways (11). We found that *Notch1* and *Sonic hedgehog (Shh)* expression was increased in ALDH^{high}, compared to ALDH^{low} cells, suggesting that the survival of ALDH^{high} cells following chemotherapy is associated with increased *Notch1* and *Shh* signaling.

Discussion

The demonstration of an association between ALDH and tumors was first shown in breast cancer (16) and subsequently in pancreatic (17), liver (18), colorectal (19), head and neck (19), thyroid (20) and lung (21) cancers. In lung cancer, ALDH activity has been shown to be selective for adenocarcinoma stem cells, depending on *Notch* signaling (21), in agreement with our observations of gastric CSCs. We demonstrated that in GC, *Notch* and *Shh* signaling may be important for both CSC maintenance and the generation of chemoresistance, providing the rationale for further study of therapy-resistant $ALDH^{high}$ CSCs. ALDH is widely used as a marker to identify and isolate various types of normal stem cells and CSCs (22). In GC, several markers reportedly characterize CSCs: CD133 (23), CD44 (23-26), side-populations identified by FACS (27), CD44 and EpCAM (25), CD54 (26) and CD90 (28). Of these markers, CD44 and ALDH are involved in aerobic glycolysis during cancer metabolism. Although an association between ALDH and the clinicopathlogical features of GC has been reported (29), the relevance of ALDH to chemoresistance has yet to be fully investigated; another study detected no association between immunohistochemical staining for ALDH and prognosis in GC patients (23). In this study, we examined for the first time the involvement of ALDH in chemoresistance and identified a candidate underlying molecular mechanism for this resistance.

GC is the second major cause of cancer-related mortality worldwide and is prevalent across Asia. *Helicobacter pylori* (*H. pylori*) infection was identified in 1982 by Marshall and Warren in patients with chronic gastritis and gastric ulcers (30). *H. pylori*-associated GC has been investigated in order to elucidate the mechanisms underlying gastric tissue damage. In general, the two mechanisms by which *H. pylori* promotes cancer are as follows: i) enhanced production of free radicals proximal to the *H. pylori* infection site, increasing the host cell mutation rate; and ii) pregenetic factors that transform host cell phenotypes by altering adhesion proteins or inflammation-related cytokines/chemokines, such as tumor necrosis factor-α or interleukin-6. Thus, *H. pylori* infection causes enhanced migration or invasion of damaged epithelial cells, without additional tumor suppressor gene mutations (31). Those non-cell autonomous mechanisms are likely facilitated by the hypoxic microenvironment of tumors, since recent studies have implicated hypoxia in inflammatory reactions provoked by *H. pylori* infection (32). Indeed, hypoxia-inducible factor-1α is mediated by the induction of a ROS-inducible protein (apurinic/apyrimidinic endonuclease 1) and its enhanced interaction with the transcriptional coactivator, p300, leads to transformed phenotypes in *H. pylori*-infected gastric epithelia (33). Although *H. pylori* infection and related atrophic gastritis are closely associated with GC, hypoxia and its related metabolism play a critical role in tumor initiation and progression in the stomach and likely in other organs (34). Further studies are warranted to elucidate the association between *H. pylori* infection and ALDH-positive CSCs in hypoxic areas and to evaluate the eradication of *H. pylori* infection and GC treatment by surgery, chemotherapy and molecular targeting of therapy-resistant CSC functions.

Acknowledgements

We thank Miyuki Ozaki and Yuko Noguchi for technical support. The current study was partly supported by a Core Research Grant-in-Aid for Scientific Research from the Ministry of Education, Culture, Sports, Science and Technology, Japan (to H.I. and M.M.); a Grant-in-Aid from the Third Term Comprehensive 10-year Strategy for Cancer Control of the Ministry of Health, Labour and Welfare, Japan (to H.I. and M.M.); a grant from the Kobayashi Cancer Research Foundation (to H.I.); a grant from the Princess Takamatsu Cancer Research Fund, Japan (to H.I.); and a grant from the SENSHIN Medical Research Foundation (to H.I.).

References

1. Bonnet D and Dick JE: Human acute leukemia is organized as a hierarchy that originates from a primitive hematopoietic cell. Nat Med 3: 730-737, 1997.
2. Reya T, Morrison SJ, Clarke MF and Weissman IL: Stem cells, cancer and cancer stem cells. Nature 414: 105-111, 2001.
3. Prince ME, Sivanandan R, Kaczorowski A, *et al*: Identification of a subpopulation of cells with cancer stem cell properties in head and neck squamous cell carcinoma. Proc Natl Acad Sci USA 104: 973-978, 2007.
4. Haraguchi N, Utsunomiya T, Inoue H, Tanaka F, Mimori K, Barnard GF and Mori M: Characterization of a side population of cancer cells from human gastrointestinal system. Stem Cell 24: 506-513, 2006.
5. Ricci-Vitiani L, Lombardi DG, Pilozzi E, Biffoni M, Todaro M, Peschle C and De Maria R: Identification and expansion of human colon-cancer-initiating cells. Nature 445: 111-115, 2007.
6. O'Brien CA, Pollett A, Gallinger S and Dick JE: A human colon cancer cell capable of initiating tumour growth in immunodeficient mice. Nature 445: 106-110, 2007.
7. Al-Hajj M, Wicha MS, Benito-Hernandez A, Morrison SJ and Clarke MF: Prospective identification of tumorigenic breast cancer cells. Proc Natl Acad Sci USA 100: 3983-3988, 2003.
8. Piccirillo SG, Reynolds BA, Zanetti N, *et al*: Bone morphogenetic proteins inhibit the tumorigenic potential of human brain tumour-initiating cells. Nature 444: 761-765, 2006.
9. Bao S, Wu Q, McLendon RE, *et al*: Glioma stem cells promote radioresistance by preferential activation of the DNA damage response. Nature 444: 756-760, 2006.
10. Ishii H, Iwatsuki M, Ieta K, Ohta D, Haraguchi N, Mimori K and Mori M: Cancer stem cells and chemoradiation resistance. Cancer Sci 99: 1871-1877, 2008.
11. Dewi DL, Ishii H, Kano Y, *et al*: Cancer stem cell theory in gastrointestinal malignancies: recent progress and upcoming challenges. J Gastroenterol 46: 1145-1157, 2011.
12. Haraguchi N, Ishii H, Mimori K, *et al*: CD13 is a therapeutic target in human liver cancer stem cells. J Clin Invest 120: 3326-3339, 2010.
13. Tamada M, Nagano O, Tateyama S, *et al*: Modulation of glucose metabolism by CD44 contributes to antioxidant status and drug resistance in cancer cells. Cancer Res 72: 1438-1448, 2012.
14. Ishimoto T, Nagano O, Yae T, *et al*: CD44 variant regulates redox status in cancer cells by stabilizing the xCT subunit of system xc(-) and thereby promotes tumor growth. Cancer Cell 19: 387-400, 2011.
15. Marcato P, Dean CA, Giacomantonio CA and Lee PW: Aldehyde dehydrogenase: its role as a cancer stem cell marker comes down to the specific isoform. Cell Cycle 10: 1378-1384, 2011.
16. Ginestier C, Hur MH, Charafe-Jauffret E, *et al*: ALDH1 is a marker of normal and malignant human mammary stem cells and a predictor of poor clinical outcome. Cell Stem Cell 1: 555-567, 2007.
17. Feldmann G, Dhara S, Fendrich V, *et al*: Blockade of hedgehog signaling inhibits pancreatic cancer invasion and metastases: a new paradigm for combination therapy in solid cancers. Cancer Res 67: 2187-2196, 2007.

18. Ma S, Chan KW, Lee TK, Tang KH, Wo JY, Zheng BJ and Guan XY: Aldehyde dehydrogenase discriminates the CD133 liver cancer stem cell populations. Mol Cancer Res 6: 1146-1153, 2008.
19. Huang EH, Hynes MJ, Zhang T, *et al*: Aldehyde dehydrogenase 1 is a marker for normal and malignant human colonic stem cells (SC) and tracks SC overpopulation during colon tumorigenesis. Cancer Res 69: 3382-3389, 2009.
20. Todaro M, Iovino F, Eterno V, *et al*: Tumorigenic and metastatic activity of human thyroid cancer stem cells. Cancer Res 70: 8874-8885, 2010.
21. Sullivan JP, Spinola M, Dodge M, *et al*: Aldehyde dehydrogenase activity selects for lung adenocarcinoma stem cells dependent on notch signaling. Cancer Res 70: 9937-9948, 2010.
22. Ma I and Allan AL: The role of human aldehyde dehydrogenase in normal and cancer stem cells. Stem Cell Rev 7: 292-306, 2011.
23. Wakamatsu Y, Sakamoto N, Oo HZ, *et al*: Expression of cancer stem cell markers ALDH1, CD44 and CD133 in primary tumor and lymph node metastasis of gastric cancer. Pathol Int 62: 112-119, 2012.
24. Takaishi S, Okumura T, Tu S, *et al*: Identification of gastric cancer stem cells using the cell surface marker CD44. Stem Cell 27: 1006-1020, 2009.
25. Han ME, Jeon TY, Hwang SH, *et al*: Cancer spheres from gastric cancer patients provide an ideal model system for cancer stem cell research. Cell Mol Life Sci 68: 3589-3605, 2011.
26. Chen T, Yang K, Yu J, *et al*: Identification and expansion of cancer stem cells in tumor tissues and peripheral blood derived from gastric adenocarcinoma patients. Cell Res 22: 248-258, 2012.
27. Fukuda K, Saikawa Y, Ohashi M, *et al*: Tumor initiating potential of side population cells in human gastric cancer. Int J Oncol 34: 1201-1207, 2009.
28. Jiang J, Zhang Y, Chuai S, *et al*: Trastuzumab (herceptin) targets gastric cancer stem cells characterized by CD90 phenotype. Oncogene 31: 671-682, 2012.
29. Katsuno Y, Ehata S, Yashiro M, Yanagihara K, Hirakawa K and Miyazono K: Coordinated expression of REG4 and aldehyde dehydrogenase 1 regulating tumourigenic capacity of diffuse-type gastric carcinoma-initiating cells is inhibited by TGF-β. J Pathol 228: 391-404 2012.
30. Marshall BJ and Warren JR: Unidentified curved bacilli in the stomach of patients with gastritis and peptic ulceration. Lancet 16: 1311-1315, 1984.
31. Suganuma M, Yamaguchi K, Ono Y, *et al*: TNF-alpha-inducing protein, a carcinogenic factor secreted from *H. pylori*, enters gastric cancer cells. Int J Cancer 123: 117-122, 2008.
32. Sinkovics JG: Molecular biology of oncogenic inflammatory processes. I. Non-oncogenic and oncogenic pathogens, intrinsic inflammatory reactions without pathogens and microRNA/DNA interactions (Review). Int J Oncol 40: 305-349, 2012.
33. Bhattacharyya A, Chattopadhyay R, Hall EH, Mebrahtu ST, Ernst PB and Crowe SE: Mechanism of hypoxia-inducible factor 1 alpha-mediated Mcl1 regulation in *Helicobacter pylori*-infected human gastric epithelium. Am J Physiol Gastrointest Liver Physiol 299: G1177-G1186, 2010.
34. Barker HE, Cox TR and Erler JT: The rationale for targeting the LOX family in cancer. Nat Rev Cancer 12: 540-552, 2012.

Bone 56 (2013) 375–382

Contents lists available at ScienceDirect

Bone

journal homepage: www.elsevier.com/locate/bone

Original Full Length Article

A human skeletal overgrowth mutation increases maximal velocity and blocks desensitization of guanylyl cyclase-B ☆

Jerid W. Robinson [a,1], Deborah M. Dickey [b,1], Kohji Miura [c], Toshimi Michigami [d], Keiichi Ozono [c], Lincoln R. Potter [a,b,*]

[a] Department of Pharmacology, University of Minnesota, Minneapolis, MN, USA
[b] Department of Biochemistry, Molecular Biology and Biophysics, University of Minnesota, Minneapolis, MN, USA
[c] Department of Pediatrics, Osaka Graduate School of Medicine, Osaka, Japan
[d] Department of Bone and Mineral Research, Osaka Medical Center and Research Institute for Maternal and Child Health, Osaka, Japan

ARTICLE INFO

Article history:
Received 18 February 2013
Revised 12 June 2013
Accepted 24 June 2013
Available online 1 July 2013

Edited by: R. Baron

Keywords:
Natriuretic peptides
Guanylate cyclase
Bone growth
cGMP
Dwarfism
Achondroplasia

ABSTRACT

C-type natriuretic peptide (CNP) increases long bone growth by stimulating guanylyl cyclase (GC)-B/NPR-B/NPR2. Recently, a Val to Met missense mutation at position 883 in the catalytic domain of GC-B was identified in humans with increased blood cGMP levels that cause abnormally long bones. Here, we determined how this mutation activates GC-B. In the absence of CNP, cGMP levels in cells expressing V883M-GC-B were increased more than 20 fold compared to cells expressing wild-type (WT)-GC-B, and the addition of CNP only further increased cGMP levels 2-fold. In the absence of CNP, maximal enzymatic activity (Vmax) of V883M-GC-B was increased 15-fold compared to WT-GC-B but the affinity of the enzymes for substrate as revealed by the Michaelis constant (Km) was unaffected. Surprisingly, CNP decreased the Km of V883M-GC-B 10-fold in a concentration-dependent manner without increasing Vmax. Unlike the WT enzyme the Km reduction of V883M-GC-B did not require ATP. Unexpectedly, V883M-GC-B, but not WT-GC-B, failed to inactivate with time. Phosphorylation elevated but was not required for the activity increase associated with the mutation because the Val to Met substitution also activated a GC-B mutant lacking all known phosphorylation sites. We conclude that the V883M mutation increases maximal velocity in the absence of CNP, eliminates the requirement for ATP in the CNP-dependent Km reduction, and disrupts the normal inactivation process.

Introduction

C-type natriuretic peptide (CNP) stimulates long bone growth and inhibits meiotic resumption in oocytes by activating the enzyme variously known as guanylyl cyclase (GC)-B, natriuretic peptide receptor (NPR)-2 or NPR-B, which catalyzes the synthesis of the intracellular signaling molecule, cGMP [1–3]. GC-B is a homodimer containing an extracellular ligand-binding domain, a single membrane-spanning region, and an intracellular highly phosphorylated kinase homology domain, dimerization domain and C-terminal GC catalytic domain [4].

CNP binding increases GC-B activity by two mechanisms. It increases the maximal rate of cGMP production called maximal velocity (Vmax) and it also increases the affinity of the enzyme for GTP that is observed as a reduction in the Michaelis constant — the GTP concentration required to reach half the Vmax. Under non-physiologic conditions such as an enzyme assay where ATP is not present, the activity of GC-B is positive cooperative as demonstrated by a Hill coefficient of greater than 1. This means that GTP binds an allosteric site that increases the affinity of the catalytic site for GTP. However, under biological conditions where ATP concentrations are at or above 1 mM, the Hill coefficient of GC-B is 1 because the allosteric site is occupied by ATP not GTP. Recently, we demonstrated that ATP is required for the CNP-dependent reduction in the Km of GC-B [5,6]. Finally, in broken cell assays, ATP also increases GC-B activity by providing the phosphate that is added to the serine and threonine residues on the enzyme that is necessary for activation by CNP [7,8].

GC-B was identified in rat chondrocytes in 1994 [9], but the ability of natriuretic peptides to stimulate skeletal growth was first observed in transgenic mice overexpressing BNP in 1998 [10]. Subsequent bone culture studies indicated that CNP, not BNP, increased the proliferative and hypertrophic zones of the murine growth plate, which increases the length of long bones [10]. CNP also increases the earliest stage of endochondral bone development – the condensation of mesenchymal precursor cells – as well as stimulates glycosaminoglycan synthesis and extracellular matrix production [11,12]. Consistent with the requirement of CNP and GC-B in normal long bone growth in mammals, mice lacking either CNP or GC-B were dwarfs [13,14], and mice lacking the

Abbreviations: CNP, C-type natriuretic peptide; GC, guanylyl cyclase; NP, natriuretic peptide; WT, wild type.

☆ Disclosure statement: The authors have nothing to declare.

* Corresponding author at: University of Minnesota — Twin Cities, 6-155 Jackson Hall, 321 Church St. SE, Minneapolis, MN 55455, USA. Fax: +1 612 624 7282.
E-mail address: potter@umn.edu (L.R. Potter).

[1] Contributed equally to this manuscript and should be considered co-first authors.

8756-3282/$ – see front matter © 2013 Elsevier Inc. All rights reserved.
http://dx.doi.org/10.1016/j.bone.2013.06.024

natriuretic peptide clearance receptor (NPR-C) that degrades CNP exhibited skeletal hyperplasia [15,16]. In contrast, mice lacking BNP display no skeletal abnormalities [17]. Importantly, CNP and CNP analogs were recently shown to increase long bone growth in murine models of achondroplasia [18–20].

Homozygous inactivating mutations in both alleles of GC-B were identified in humans with acromesomelic dysplasia, type Maroteaux (AMDM) dwarfism [21–23], and heterozygous mutations in GC-B were associated with non-pathological reductions in human stature [24]. Conversely, mutations associated with CNP overexpression were identified in patients with skeletal overgrowth [25,26], and a genome-wide association study identified correlations between genetic mutations that regulate CNP or NPR-C expression and height in Northwestern European populations [27].

In 2012, Miura et al. identified a conserved valine to methionine missense mutation at position 883 in the catalytic domain of human GC-B (V883M-GC-B) in three generations of a Japanese family with skeletal overgrowth, fragile bones and elevated blood cGMP concentrations [28]. Importantly, how this mutation increases GC-B activity was not determined. Here, we show that this single residue substitution increases the maximal velocity of GC-B in the absence of CNP and that CNP reduces the Km of V883M-GC-B an order of magnitude without ATP or without increasing maximal velocity. Unexpectedly, the V883M substitution blocked the normal inactivation process.

Materials and methods

Reagents

^{125}I-cGMP radioimmunoassay kits and ^{32}P-α-GTP were from Perkin Elmer (Waltham, MA). CNP-22 was purchased from Sigma (St. Louis, MO). The plasmids encoding the N-terminally HA-tagged form of WT human GC-B (HA-WT-GC-B) [22] and HA-V883M-GC-B plasmids [28] have been described. The plasmids expressing rat GC-B-7A and GC-B-7E were also previously described [29,30]. The ATDC5 chondrocytes were from ATCC (www.atcc.org).

Cells and transfections

293 neocells were maintained and transiently transfected by the HEPES–calcium-phosphate precipitation method as previously reported [30].

Whole cell cGMP elevation assays

Cyclic GMP concentrations were measured by radioimmunoassay in ethanol extracts of transiently transfected 293 cells that were pre-incubated with 1 mM isobutylmethyl xanthine, a general phosphodiesterase inhibitor, for 10 min before being incubated with increasing concentrations of CNP as previously described [31].

Guanylyl cyclase assays

Crude membranes were prepared at 4 °C in phosphatase inhibitor buffer consisting of 50 mM 4-(2-hydroxyethyl)-1-piperazineethanesulfonic acid — pH 7.4, 50 mM NaCl, 20% glycerol, 50 mM NaF, 1 mM EDTA, 0.5 μM microcystin and 1× Roche protease inhibitor cocktail. All assays were performed at 37 °C in a cocktail containing 25 mM HEPES pH 7.4, 50 mM NaCl, 0.1% BSA, 0.5 mM isobutylmethyl xanthine, 1 mM EDTA, 0.5 μM microcystin, 5 mM phosphocreatine, 0.1 μg/μl creatine kinase and 5 mM $MgCl_2$.

The single substrate concentration GC assays were performed using ^{32}P-GTP as substrate in the presence of 1 mM ATP and 1 mM GTP at 37 °C for 3 min as previously described [31]. For the desensitization assays, the reaction was performed using a pool of crude membranes. The reaction was initiated by the addition of pre-warmed cocktail. At the designated times, 0.1 ml aliquots were removed and added to ice-cold tubes containing 0.5 ml zinc acetate to stop the reaction. Alumina column chromatography purified the ^{32}P-cGMP, which was quantified by Cerenkov counting [32].

Substrate-velocity assays were performed for the indicated times with the indicated GTP concentrations. The resulting cGMP concentrations were determined by radioimmunoassay as described [33]. When included, free manganese concentrations in the assays were 2 mM. Because enzymatic activity was not completely linear with time, the kinetic parameters obtained under these conditions are considered "apparent".

Western blotting

293T cells were transfected with the indicated constructs, immunoprecipitated, fractionated by reducing SDS-PAGE and blotted to an Immobilon membrane for immune-detection as previously described [34]. The blot was blocked and probed with at 1/2500 dilution of rabbit serum 6328 followed by incubation with a 1/20,000 dilution of goat anti-rabbit IRDye 680 conjugated antibody and visualized on a LI-COR instrument as previously described [35].

Statistical analysis

Statistics and graphs were generated with Prism 5 software. Student's paired *t*-test determined significance where $p \leq 0.05$ was considered significant. The vertical bars within the symbols represent the SEM. Where not visible the bars are contained within the symbol. EC_{50} values were calculated based on the nonlinear curve fitting equation $Y = Top * X / (EC_{50} + X)$. Substrate–velocity curves were analyzed using an allosteric sigmoidal model to generate Hill coefficients.

Results

Cyclic GMP is elevated more than twenty-fold in cells expressing GC-B-V883M

HEK293 cells were transiently transfected with human isoforms of HA-WT-GC-B or HA-V883M-GC-B. Two days later, the cells were incubated in the presence of increasing concentrations of CNP for 3 min and intracellular cGMP concentrations were determined (Fig. 1A). Basal (no CNP) cGMP concentrations were elevated 21-fold in cells expressing HA-V883M-GC-B compared to cells expressing HA-WT-GC-B. Maximal concentrations of CNP increased cGMP concentrations 29-fold in HA-WT-GC-B expressing cells but only 2-fold in cells expressing HA-V883M-GC-B. The EC_{50} for CNP activation was not significantly different between the WT and mutant enzymes, consistent with the mutation not affecting the affinity of CNP for GC-B.

Plasmids expressing WT and GC-B-V883M were also transiently transfected into ATDC5 mouse chondrocytic cells that endogenously express GC-B. Since these cells express phosphodiesterases 1 and 5, we pretreated them with a general phosphodiesterase to emphasize cGMP synthesis by GC-B [36]. Overexpression of WT-GC-B slightly elevated cyclic GMP concentrations in the ATDC5 cells, but overexpression of the GC-B-V883M mutant resulted in cGMP levels that were more than four-fold higher than those observed in cells transfected with the WT enzyme (Fig. 1B). These data indicate that the increased basal activity associated with the V883M mutation occurs in a natural cellular environment for GC-B and is consistent with the increased plasma cGMP concentrations measured in patients expressing V883M-GC-B [28].

Basal enzymatic activity of V883M-GC-B is elevated but expression is reduced

GC activity was measured in crude membranes from 293 cells expressing green fluorescent protein (GFP) as a control, WT-GC-B,

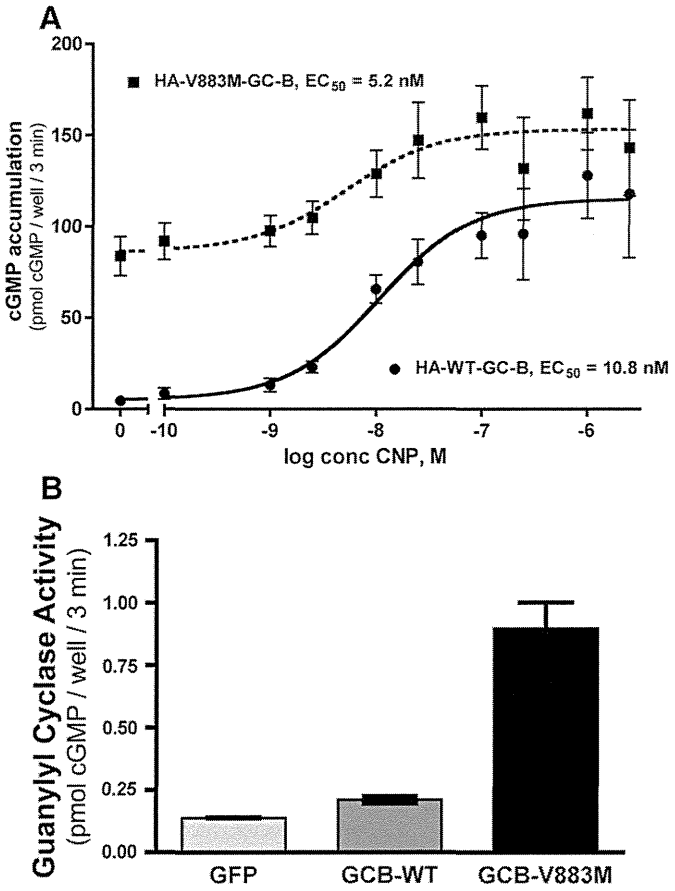

Fig. 1. Basal cGMP concentrations are markedly elevated in cells expressing V883M-GC-B. A, 293 cells transiently expressing HA-WT-GC-B or HA-V883M-GC-B were incubated with the indicated concentrations of CNP for 3 min and then intracellular cGMP concentrations were determined. The EC_{50}s for the two enzymes were not significantly different, $p = 0.42$. B, ATDC5 cells were transiently transfected with plasmids expressing WT-GC-B or GC-B-V883M and cGMP concentrations were measured in basal (no CNP) serum-starved cells 2 days later. Cyclic GMP concentrations in cells expressing WT-GC-B were slightly higher than those observed in un-transfected cells ($p < 0.01$), but levels in cells expressing GC-B-V883M were 4.3-fold higher than those in cells expressing WT-GC-B ($p < 0.03$).

HA-WT-GC-B or HA-V883M-GC-B under basal (1 mM Mg^{2+}GTP), hormone-stimulated (1 mM Mg^{2+}GTP, 1 mM ATP and 1 μM CNP), or detergent-stimulated (1 mM Mn^{2+}GTP and 1% Triton X-100) condition (Fig. 2). Enzyme analysis was performed in the 293 cells because they do not express detectable endogenous GC activity [6], which allows more definitive interpretation of the data because most tissues and cell lines express more than one GC.

GC activity measured in crude membranes from GFP transfected cells was insignificant under all conditions. Consistent with the whole cell cGMP analysis describe in Fig. 1, basal GC activity was low for WT-GC-B and HA-WT-GC-B but was elevated 28-fold over WT levels for HA-V883M-GC-B. Saturating concentrations of CNP and ATP stimulated WT-GC-B and HA-WT-GC-B similarly (>50-fold). However, GC activity of HA-WT-GC-B was almost double that of the WT enzyme lacking the HA tag, consistent with higher expression of the HA-tagged receptor. As in whole cells, CNP and ATP activated HA-V883M-GC-B about two-fold in enzyme assays. GC activity of HA-V883M-GC-B measured in the presence of detergent was lower than that observed for HA-WT-GC-B, which is consistent with reduced expression of HA-V883M-GC-B compared to HA-WT-GC-B. Western analysis of SDS-PAGE fractionated immunoprecipitated enzymes confirmed that the more slowly migrating, completely processed species (upper band) was expressed at lower levels than the comparably processed forms of the tagged or untagged WT version of GC-B (Fig. 2, inset). We previously

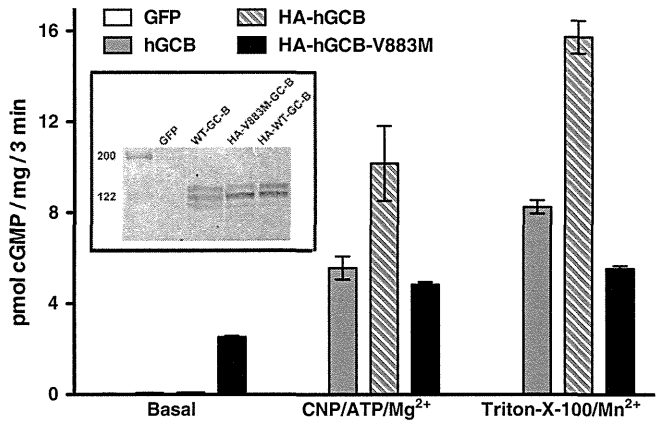

Fig. 2. GC activity but not the protein level of V883M-GC-B was elevated in the absence of CNP. Crude membranes from 293 cells transfected with plasmids expressing the indicated constructs were assayed for GC activity under the conditions indicated in the figure legend and text. Bars within the symbols indicate the range of duplicate determinations. This figure is representative of two independent assays. The inset shows a Western blot of the indicated forms of GC-B purified from 293 cells transiently transfected with the indicated constructs. The numbers on the left indicate the molecular weight of standards.

demonstrated that only the upper band of GC-B is phosphorylated and that phosphorylation is required for CNP-dependent activation of GC-B [8,29].

Maximal velocity of HA-GC-B-V883M is elevated

To determine how the mutation increased the enzymatic activity of GC-B, substrate–velocity curves were generated for HA-WT-GC-B and HA-V883M-GC-B with or without 1 μM CNP in the absence of ATP (Fig. 3A). Basal activity of the WT enzyme was low and CNP increased Vmax 12-fold without decreasing the Km. Consistent with previous observations [6], WT-GC-B was positive cooperative as indicated by a Hill slope of 1.3. In contrast, basal maximal velocity of the mutant enzyme was elevated 15-fold compared to WT-GC-B and the Km was unchanged. The Hill coefficient was 0.9, suggesting slight negative cooperativity. CNP failed to increase the maximal velocity of HA-V883M-GC-B, but reduced the Hill slope 0.4 units and the Km 10-fold. Thus, the V883M mutation increases basal maximal velocity, reduces the Hill coefficient and allows CNP to reduce the Km in the absence of ATP. In contrast, the reduction in Hill coefficient and Km for the WT enzyme was previously shown to be completely dependent on the presence of ATP [5]. These data are consistent with the V883M mutation producing a structural change in GC-B that locks it into a conformation that mimics that of the ATP-bound state. They also indicate for the first time that the CNP-dependent changes in the Vmax and Km of GC-B are separate but related processes.

CNP reduces the Hill coefficient and Km of HA-V883M-GC-B in a concentration-dependent manner in the absence of ATP

Substrate–velocity curves were generated for HA-V883M-GC-B in the presence of increasing concentrations of CNP to evaluate the concentration-dependence of CNP on reductions in the Hill coefficient and Michaelis constant (Fig. 3B). ATP was not included in these experiments. In the absence of CNP, no cooperativity was observed, but increasing concentrations of CNP progressively increased the amount of negative cooperativity while concomitantly decreasing the Km. These data indicate that CNP converts HA-V883M-GC-B to a strongly negative cooperative enzyme. Similarly, in the absence of CNP, the Km of the mutant enzyme was high; but in the presence of increasing concentrations of CNP, the Km dropped progressively while maximal velocity was unaffected.

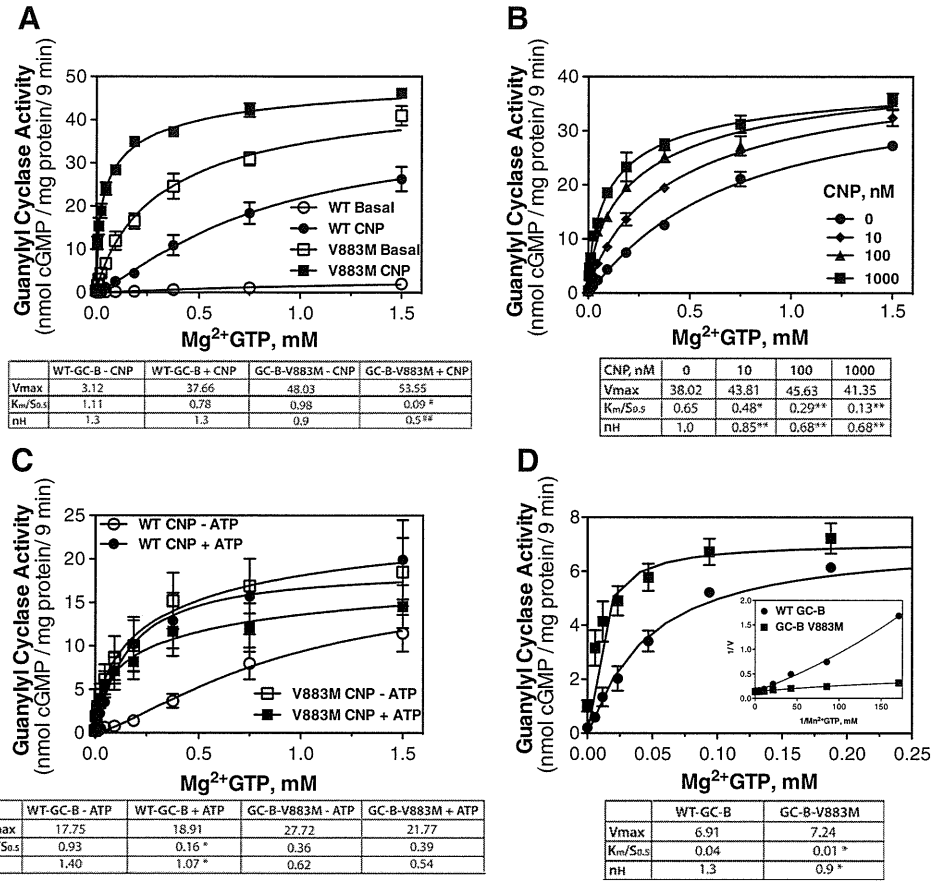

	WT-GC-B - CNP	WT-GC-B + CNP	GC-B-V883M - CNP	GC-B-V883M + CNP
Vmax	3.12	37.66	48.03	53.55
$K_m/S_{0.5}$	1.11	0.78	0.98	0.09 #
nH	1.3	1.3	0.9	0.5 ##

CNP, nM	0	10	100	1000
Vmax	38.02	43.81	45.63	41.35
$K_m/S_{0.5}$	0.65	0.48*	0.29**	0.13**
nH	1.0	0.85**	0.68**	0.68**

	WT-GC-B - ATP	WT-GC-B + ATP	GC-B-V883M - ATP	GC-B-V883M + ATP
Vmax	17.75	18.91	27.72	21.77
$K_m/S_{0.5}$	0.93	0.16 *	0.36	0.39
nH	1.40	1.07 *	0.62	0.54

	WT-GC-B	GC-B-V883M
Vmax	6.91	7.24
$K_m/S_{0.5}$	0.04	0.01 *
nH	1.3	0.9 *

Fig. 3. Kinetic characterization of V883M-GC-B. GC activity shown in panels A–D was measured for 9 min in crude membranes from 293 cells transiently expressing either HA-GC-B-WT or HA-GC-B-V883M. Bars within symbols indicate the SEM. Tables below each figure show Vmax, Km and Hill coefficient (n_H). A. Maximal velocity of HA-V883M-GC-B is elevated in the absence of CNP. GC activity was measured in the presence or absence of 1 μM CNP and the indicated concentrations of $Mg^{2+}GTP$ where n = 4. The # indicates a significant difference from HA-WT-GC-B-CNP at $p < 0.05$. The ## indicates a significant difference from HA-V883M-GC-B-CNP at $p < 0.03$. B. CNP decreases the Hill coefficient and Km for HA-V883M-GC-B in a concentration-dependent manner in the absence of ATP. GC activity was measured in the presence or absence of increasing concentrations of CNP and the indicated concentrations of $Mg^{2+}GTP$ where n = 4. * and ** indicate a significant difference from no CNP values where $p < 0.05$ and 0.01, respectively. C. ATP does not affect the Hill coefficient or Km of HA-V883M-GC-B. GC activity was measured in the presence or absence of 0.1 mM ATP, 1 μM CNP and the indicated concentrations of $Mg^{2+}GTP$ where n = 4. The * indicates a significant difference from HA-WT-GC-B (−) ATP at $p < 0.05$. D. HA-V883M-GC-B is negative cooperative. GC activity was measured with the indicated concentrations of $Mn^{2+}GTP$ and 1% Triton X-100 where n = 6. The * indicates a significant difference from the corresponding value obtained for the WT enzyme at $p < 0.05$; inset. Double reciprocal plots were generated from the raw data to demonstrate a concave upward curve indicative of positive cooperativity or a slightly downward curve indicative of negative cooperativity.

ATP does not allosterically activate V883M-GC-B

We recently determined that CNP reduces the Hill coefficient and Km of WT-GC-B by a process that requires ATP binding to an allosteric site in the catalytic domain [6]. Therefore, we investigated whether the V883M mutation affected these processes as well. Substrate–velocity curves were generated for HA-WT-GC-B and HA-V883M-GC-B in the presence of 1 μM CNP with or without 0.1 mM ATP. With the WT enzyme, ATP reduced the Km 6-fold and the Hill coefficient 0.3 units without affecting the Vmax (Fig. 3C). However, ATP failed to reduce the Km or Hill coefficient or increase the Vmax of HA-V883M-GC-B. These data are consistent with a scenario where the V883M mutation causes a conformational change in GC-B that abolishes the need for ATP in the CNP-dependent reduction in Hill coefficient and Km.

HA-V883M-GC-B is slightly negative cooperative when manganese is used as a cofactor

Substrate–velocity curves were also generated on membranes expressing HA-WT-GC-B or HA-V883M-GC-B under non-physiologic, detergent conditions using manganese-GTP as substrate (Fig. 3D). Substrate–velocity curves generated under these conditions were previously shown to be positive cooperative for GC-A [37]. Vmax was lower when measured under these conditions but the Km/S0.5 was strikingly lower compared to physiologic activation conditions. Maximal velocity was not different between the WT and mutant GC-B enzymes. The substrate–velocity curve for HA-WT-GC-B was positive cooperative as demonstrated by concave upward reciprocal plots and a Hill coefficient of 1.3 (Fig. 3D, inset). To our knowledge, this is the first demonstration of positive cooperativity for GC-B when assayed under detergent-stimulated conditions. In contrast to HA-WT-GC-B, HA-V883M-GC-B was weakly negative cooperative as indicated by a slightly concave downward curve and a Hill coefficient of 0.9 (Fig. 3D, inset), which is consistent with the slight negative cooperativity observed for V883-GC-B when assayed under basal conditions.

HA-V883M-GC-B is resistant to desensitization

Cyclic GMP concentrations in cells expressing V883M-GC-B were highly elevated two days after transfection (Fig. 1), which suggests that the mutant enzyme was not completely desensitized or downregulated. In contrast, CNP activated WT-GC-B was shown to desensitize in less than one hour [8]. Therefore, we examined whether the V883M mutation disrupted the inactivation of GC-B.

GC activity was measured on membranes from cells expressing HA-WT-GC-B or HA-V883M-GC-B for up to 2 h to evaluate the effect of the V883M mutation on the inactivation of GC-B as a function of time (Fig. 4, top panel). WT GC activity was determined in the